Modelling the diurnal and seasonal dynamics of soil CO_2 exchange in a semiarid ecosystem with high plant-interspace heterogeneity

Jinnan Gong[1], Ben Wang [1,2], Xin Jia[1,2], Wei Feng[2], Tianshan Zha[2], Seppo Kellomäki[1] and Heli Peltola[1]

[1] School of Forest Sciences, University of Eastern Finland, P.O. Box 111, 80101 Joensuu, Finland

[2] Yanchi Research Station, School of Soil and Water Conservation, Beijing Forestry University, Beijing 100083, China

Correspondence to: Jinnan Gong (jinnan.gong@uef.fi)

Abstract

In this study we investigated i) the roles of different C-flux components in regulating soil CO_2 exchanges (F_S) in a dryland ecosystem of high plant-interspace heterogeneity, and ii) plant-interspace differences in the C flux components. A process-based approach was used to model the diurnal and seasonal dynamics of F_S, which considered simultaneously the CO_2 production, transport and surface exchanges (e.g. biocrust photosynthesis, respiration and photodegradation). The model was parameterized and validated with multivariate data measured during year 2013-2014 in a semiarid shrubland ecosystem in Yanchi, northwestern China. The model explained reasonably well the F_S dynamics measured from a non-crusted and two lichen-crusted plots during a two-year period. The model simulation showed that, soil rewetting could enhance CO_2 dissolution and delay the emission of CO_2 produced from root-zone. In addition, an ineligible fraction of respired CO_2 might be removed from soil volumes under respiration chambers by lateral water flow and root uptake. During rewetting, the lichen-crusted soil could shift temporally from net CO_2 source to sink, due to the photosynthesis of lichens and restricted CO_2 emissions from subsoil. The presence of plant cover could decrease the root-zone CO_2 production and biocrust C sequestration, but increase the temperature sensitivities of these fluxes. On the other hand, the sensitivities of root-zone emissions to water content were decreased by canopy, which may be due to the advection of water flows from the interspace. To conclude, the complexity and plant-interspace heterogeneities of soil C processes should be carefully considered to extrapolate findings from chamber to ecosystem scales, and to predict the ecosystem responses to climate change and extreme climatic events. Our model can serve as a useful tool to simulate the soil CO_2 efflux dynamics in dryland ecosystems.

Keyword: ecosystem modelling; heterogeneity; inorganic carbon; semiarid shrub ecosystem; biocrust

1. Introduction

The CO_2 exchange between soil and atmosphere constitutes a major C loss from terrestrial ecosystems (Raich et al., 2002; Giardina et al., 2014). It also plays an important role in the feedbacks between global carbon cycle and climate change (Rustad et al., 2000; Giardina et al., 2014; Karhu et al., 2014). Arid and semiarid (dryland) ecosystems cover over 40% of land surface and contribute notably to inter-annual variations of terrestrial C sink (Poulter et al., 2014). However, the contribution of soil CO_2 flux (F_S) from those ecosystems to the global C budget is less-studied (Castillo-Monroy et al., 2011; Gao et al., 2012; Jia et al., 2014). The temperature dependency of biological CO_2 production (i.e. autotrophic respiration and heterotrophic respiration) serves a conventional basis for F_S modelling in many terrestrial ecosystems (Raich and Tufekciogul, 2000; Ryan, 2005; Song et al., 2015). Soil CO_2 flux of dryland ecosystems is also widely interpreted using temperature-response functions modified by other environmental constraints, e.g. soil water content, abundances of substrates and microbial activities (Curiel Yuste et al., 2007; Wang et al., 2014a, 2014b, 2015).

Although many empirical studies have explained the dynamics of soil CO_2 flux in specified space-time, their lack of mechanistic descriptions represents a major difficulty in extrapolation under changing environmental conditions (Fan et al., 2015). Soil CO_2 flux is a "bulk" exchange that comprises two main sets of processes, i.e. the CO_2 production and transport (Fang and Moncrieff, 1999; Fan et al., 2015). Hence, models considering only autotrophic and heterotrophic respiration often fail to account for the observed F_S dynamics (Austin and Vivanco, 2006). Gas transport processes are important mechanisms regulating the magnitude and hysteretic feature of soil CO_2 efflux (Ma et al., 2013). A substantial fraction of respired CO_2 may be transported to atmosphere via xylem, and may not be measured by techniques like soil reparation chambers (Bloemen et al., 2013; 2016). During wet periods, soil CO_2 efflux could decrease significantly by water clogging of soil pores, which restricts the diffusion of O_2 and CO_2 gases (Šimunek and Suarez, 1993; Fang and Moncrieff, 1999). In dryland soils of high salinity/alkalinity, CO_2 transport and water cycle are tightly coupled, as large inorganic C fluxes can be driven solely by dissolution and infiltration of CO_2 and carbonates (Buysse et al., 2013; Ma et al., 2013; Fa et al., 2014). Such inorganic transport may not only introduce fluctuations to hourly or diurnal soil CO_2 efflux (e.g. Emmerich, 2003; Xie et al., 2009; Buysse et al., 2013), it may also to terrestrial CO_2 sinks at much broader spatiotemporal scales (Schlesinger, 2009; Li et al., 2015).

Key processes contributing to CO_2 production in dryland soils also extend beyond autotrophic respiration and heterotrophic respiration. Although biocrust organisms (lichens, mosses, bacteria, fungi and microfauna) inhabit in the top few centimetres of the soil profile, they constitute up to 70% of biomes in interspace areas (Belnap, 2003). These communities are able to uptake C from the

atmosphere (Belnap, 2003; Castillo-Monroy et al., 2011; Maestre et al., 2013), leading to largely greater concentration of organic matter in the crusted layer than the soil underneath (Ciais et al., 2013). Although crust organisms could be inactive under stresses (e.g. drought, Green and Proctor, 2016), their photosynthetic potential could be large (Zaady et al., 2000; Lange, 2003), even comparable to temperate forests with closed canopies (e.g. Zaady et al., 2000). The net C uptake by biocrust is highly sensitive to stresses like droughts, thermal extremes and excessive ultraviolet radiation (Pointing and Belnap, 2012). Such variations can readily alter the crusted soils between considerable CO_2 sinks and sources within a few hours (e.g. Bowling et al., 2011; Feng et al., 2014). In addition, the accumulation of debris from crust and canopy fuels photodegradation, which represents an important abiotic C loss in arid conditions beside the biotic decomposition (e.g. Austin and Vivanco, 2006; Throop et al., 2009). Photodegradation is likely to dominate the mineralization during dry daytime periods, when radiation is strong and microbial activities are prohibited by low moisture content and high temperature (e.g. Gliksman et al., 2016). On an annual basis, photodegradation could consume more than 10% of soil organic matter (SOM) at surface (e.g. Austin and Vivanco, 2006; Henry et al., 2008; Brandt et al., 2010), even for the substrates (e.g. lignin) that are difficult to degrade via biotic pathways (Henry et al., 2008).

The influences of multiple C processes (i.e. autotrophic and heterotrophic respiration, net C uptake by biocrust, inorganic C fluxes and photodegradation) on soil CO_2 exchange are highly overlapped and tightly related to the water-energy processes. In dryland ecosystems, patchy vegetation and large fractions of interspace are common features (Domingo et al., 2000), and the water-thermal conditions can vary considerably from plant cover to interspace even within a few meters (Rodríguez-Iturbe et al., 2001; Caylor et al., 2008; Ma et al., 2011). The water-energy dynamics at the different surfaces are linked by multiple advection processes both above- and below-ground (Gong et al., 2016). Due to the complexity of water-energy processes, there may exist possibly high non-linearity of water-thermal responses to the climatic variability (e.g. Phillips et al., 2011; Barron-Gafford et al., 2013). This will also complicate the C responses and consequently affect the relationships between the CO_2 fluxes and environmental controls (e.g. Jarvis et al., 2007; Song et al., 2015).

Global climate change is expected to increase annual mean air temperature considerably and alter precipitation regimes (Donat et al., 2016). Understanding the response of dryland ecosystems to such changes requires mechanistic models that integrate the multiple biotic and abiotic mechanisms in soil C cycling. So far, only a few models have coupled the biotic CO_2 production with the transport of gas and heat (Šimunek and Suarez, 1993; Fang and Moncrieff, 1999; Phillips et al., 2011; Ma et al., 2013; Fan et al., 2015). Nevertheless, none of those models has described the heterogeneous water-energy processes in soil-vegetation-atmosphere continuum (SPAC), or the unconventional C fluxes such as net C uptake by biocrust and photodegradation despite the importance of these processes in arid and semiarid environments. Perhaps, models by Porada et al. (2013) and Kinast et al. (2016) represent the

few existing works in this sense. However, both the models focus on the patterns at the regional-scale with very simplified ecosystem processes.

The aims of this study are: i) to investigate the roles of soil CO_2 components in regulating soil CO_2 effluxes in the studied ecosystem, and ii) to estimate the plant-interspace differences in the componential C processes. For these purposes, we developed a process-based model, which considered simultaneously the CO_2 production, transport and surface exchanges (e.g. biocrust photosynthesis, respiration and photodegradation). Based on the water-energy modelling of Gong et al. (2016), the model development focused on the CO_2 production and transportation in root-zone soil, and the C exchanges driven by surface processes, such as biocrust metabolism and photodegradation. The model was run at half-hourly time step to capture the responses of soil CO_2 effluxes to rain pulses and diurnal variations of radiation and thermal conditions. The model was parameterized and validated by multi-variant data measured during year 2013-2014 in a semiarid shrubland ecosystem in Yanchi, northwestern China. A series of sensitivity analysis were then carried to study the effects of stand-scale heterogeneities and the complexity of soil C processes in regulating the soil CO_2 exchanges in the dryland ecosystem.

2. Materials and methods

2.1 Model overview

The process-based model was build based on semiarid shrubland ecosystem located at the southern edge of the Mu Us desert (37°42'1" N, 107°13'7" E, 1560 m above sea level, Fig. 1a), Ningxia, China (see Wang et al., 2014a, 2015). The long-term mean temperature (1954–2004) is 8.1 °C, and the mean annual precipitation is 287 mm, most of which falls from July to September (Jia et al., 2014). The radiation and evaporation demand are high in this area, i.e. the annual incoming shortwave radiation is 1.4×10^5 J cm^{-2} and the annual potential evaporation is 2024 mm. The vegetation is dominated by scattered crowns of *Artemisia ordosica* (Fig. 1b). The soil is highly alkaline (pH = 8.2). Biocrust (mainly lichens and algae) covers about 40% of interspace soil (Fig. 1c - 1e). The thickness of the crust layer was 0.5 – 2.5 cm (Gong et al., 2016).

In the modelling, the structure of ecosystem was considered as replications of "representative land units" (RLU, Fig. 1f; Gong et al., 2016), which comprises the area covered by shrubs and the surrounding soil (interspace). Vertically, the model simulates the C flows over the soil profile and the water-energy transport from the lower boundary of rooting zone to a reference height in the boundary atmosphere. Horizontally, the SPAC processes at plant cover and the surrounding interspace are differentiated but related via advection and diffusion flows, as driven by the gradients of temperature,

water potential and gas concentrations. The mineralization, uptake and transport of soil C and N are further regulated by water-energy conditions.

Fig. 2 shows the framework of key processes and variables included in the F_S modelling. The model includes a set of sub-models, which describe: (i) CO_2 dissolution, transport and efflux; (ii) Autotrophic and heterotrophic CO_2 production in the soil profile; (iii) CO_2 uptake and emission by biocrust; (iv) Surface energy balance and soil temperature profile; and (v) Soil hydrology and water balance. These sub-models are linked by multiple feedbacks to represent the coupling of C, water, vapor and energy transportations in the ecosystem. Sub-models (iv) - (v) have been developed and described in details in our previous work (Gong et al. 2016), which focused on (i) introducing the plant-interspace heterogeneity into water-energy modelling, and (ii) investigating the influences of such heterogeneity on the ecosystem water-energy budgets for a dryland ecosystem. Gong et al. (2016) also validated the model in regard to the diurnal to seasonal dynamics of radiation balance, surface energy balance, soil temperature and moisture content in the footprint area of a eddy-covariance (EC) site (details of measurement see Jia et al., 2014). In this work, we therefore focused on the development of sub-models (i) – (iii) and their parameterization and validation by F_S measurements, based on automatic respiration chambers from crust-covered and non-crusted soils. Based on the validated model, we also analyzed the model sensitivities to stand parameters and plant-interspace heterogenity and investigated the relative contribution of different flux components to F_S.

2.2 Modelling approaches

2.2.1 Submodel (i): CO_2 transport, dissolution and efflux

For soil fraction x (see Fig. 1f for RLU settings), CO_2 exchange (F_S, upward positive) was the sum of CO_2 exchange by biocrust (F_{Ct}), photodegradation (F_P) and the emission from soil under the biocrust layer (F_T):

$$F_{S_x} = F_{Ct_x} + F_{T_x} + F_{P_x} \quad (1)$$

where F_{Ct} is the net balance between biocrust photosynthesis (P_{Ct}) and respiration (R_{Ct}), and $F_{Ct} = P_{Ct} - R_{Ct}$ (see Section 2.2.3). F_T was modelled based on the mass-balance functions developed by Fang and Moncrieff (1999), and combined major transport processes in both gaseous and liquid phases. To account for the plant-interspace heterogeneity, we expanded the original one-dimensional function to the two-dimensional space. For soil layer (x, i) and time step t, the CO_2 concentration and C flows were calculated as follows:

$$\frac{\partial C_{x,i}}{\partial t} = \frac{\partial}{\partial Z}\left(F_{dg}^{v} + F_{ag}^{v} + F_{dw}^{v} + F_{aw}^{v}\right) + \frac{\partial}{\partial h}\left(F_{dg}^{h} + F_{ag}^{h} + F_{dw}^{h} + F_{aw}^{h}\right) + S_{x,i} \quad (2)$$

where superscripts *v* and *h* denote the vertical and horizontal directions, respectively (see also in Gong et al., 2016); *C* is the total CO_2 content; F_{dg} and F_{dw} are the CO_2 flows due to diffusion/dispersion via the gaseous and liquid phases; F_{ag} and F_{aw} are the flows in gaseous and liquid phases due to gas convection and water movement, and *S* is the net CO_2 sink of the layer. The calculation schemes of F_{dg}, F_{dw}, F_{ag} and F_{aw} have been described in detail by Fang and Moncrieff (1999). F_T is the total exchange of gaseous CO_2 between surface and topmost layer:

$$F_{T_x} = F^v_{dg_{x,1}} + F^v_{ag_{x,1}} + E^S_{x,1} C_{w_{x,1}} \quad (3)$$

where $E^S_{x,1}$ is the soil evaporation at section *x* (see Eq. (17) in Gong et al., 2016); C_w is the equivalent CO_2 concentrations in the solution of the topmost soil. For layer (*x*, *i*), C_w is linked to the gaseous CO_2 concentrations (C_g):

$$C_{x,i} = Cg_{x,i}\left(V_{x,i} - \theta_{x,i}\right) + Cw_{x,i}\theta_{x,i} \quad (4)$$

where *V* is the total porosity; and θ is soil water content.

C_g and C_w were further related via the dissolution-dissociation balance of CO_2 in soil solution, following Fang and Moncrieff (1999) and Ma et al (2013):

$$CO_2(g) + H_2O(l) \rightleftarrows H_2O(l) + CO_2(aq) \quad K_H = P_C/CO_2^{aq} \quad (5)$$

$$CO_2(aq) + H_2O(l) \rightleftarrows H_2CO_3 \quad K_0 = CO_2^{aq}/[H_2CO_3] \quad (6)$$

$$H_2CO_3 \rightleftarrows [H^+] + [HCO_3^-] \quad K_1 = [H^+][HCO_3^-]/[H_2CO_3] \quad (7)$$

$$HCO_3^- \rightleftarrows [H^+] + \left[CO_3^{2-}\right] \quad K_2 = [H^+]\left[CO_3^{2-}\right]/[HCO_3^-] \quad (8)$$

where P_C is the partial pressure of CO_2 in pore air; K_H is Henry's Law constant; K_0, K_1 and K_2 are equilibrium coefficients of dissolution, the first- and the second-order dissociation reaction for carbonic acid, respectively (for details see Fang and Moncrieff, 1999). The equilibrium $[H^+]$ was determined by the soil pH and the coefficients K_H, K_0, K_1 and K_2, which were functions of soil temperature in each soil layer (Fang and Moncrieff, 1999). *Cw* was calculated as the sum of CO_2^{aq}, H_2CO_3, HCO_3^- and CO_3^{2-}.

2.2.2 Submodel (ii): autotrophic and heterotrophic CO_2 production along the soil profile

For soil layer (*x*, *i*), $S_{x,i}$ (Eq. 2) was calculated as the sum of autothrophic and heterotrophic CO2 production, and the dissolved CO_2 removed with the water uptaken by roots:

$$S_{x,i} = Rs_{x,i} + Ra_{x,i} - E_{x,i} Cw_{x,i} \quad (9)$$

where *E* is the transpirative uptake of water (Gong et al., 2016); *Rs* is the CO_2 production by heterotrophic SOM decomposition; *Ra* is the autotrophic respiration of the rhizosphere, which comprises maintenance respiration (*Rm*) and growth respiration (*Rg*):

$$Ra_{x,i} = Rm_{x,i} + Rg_{x,i} \quad (10)$$

To simulate *Rs*, we simplified the pool-type model of Gong et al (2013, 2014), which was originated from Smith et al (2010) for simulating coupled C and N cycling in organic soils. SOM pool in each soil layer was divided into debris (M_{deb}, i.e. litters from roots and biocrust), microbes (M_{mic}) and humus (M_{hum}), which are different in biochemical recalcitrance and N content. During decaying, mineralized masses transfer from M_{deb} and M_{mic} to more resistant form (i.e. M_{hum}), leading to a decrease in lability (e.g. Li et al., 1992). The mineralization of organic C followed first-order kinetics and was constrained by multiple environmental multipliers, including temperature, water content and oxygen content (Šimunek and Suarez, 1993; Fang and Moncrieff, 1999):

$$m_{x,i}^{r} = M_{x,i}^{r} k_r f(Ts_{x,i}) f(\theta_{x,i}) f(O_{x,i}) dt \quad (11)$$

where superscript *r* denotes the type of SOM pool (r=1 for M_{deb}, r=2 for M_{mic}, and r=3 for M_{hum},); *m* is mineralized SOM during time step *dt*; *k* is the decomposition constant; *dt* is time step; $f(Ts_{x,i})$, $f(\theta_{x,i})$ and $f(O_{x,i})$ are multiplier terms regarding the temperature, water content and oxygen restrictions, respectively. $f(O_{x,i})$ was calculated following Šimunek and Suarez (1993). $f(Ts_{x,i})$ and $f(\theta_{x,i})$ were reparameterized with respect to the site-specific conditions of plants and soil (see section 2.4.3). The CO_2 production from mineralization was further regulated by the N-starvation of microbes following Smith et al. (2010):

$$Rs_{x,i} = r_E m_{x,i}^{r} \quad (12)$$

where r_E is the gas production rate ($r_E \epsilon$ [0, 1]), and (1- r_E) is the proportion of organic matters passed to the downstream SOM pools. The evolution of each SOM pool was calculated as below:

$$M_{x,i}^{r} = (1 - r_E) m_{x,i}^{r-1} - m_{x,i}^{r} + A_{x,i}^{r} dt \quad (13)$$

where *A* is the SOM input rate (A=0 for M_{mic} and M_{hum}); superscript *r*-1 denotes the source SOM pools.

$Rm_{x,i}$ was calculated in a similar way to $Rs_{x,i}$ (e.g. Chen et al., 1999; Fang and Moncrieff,1999). $Rg_{x,i}$ was calculated as a fraction of photosynthetic assimilates, following Chen et al. (1999):

$$Rm_{x,i} = M_{x,i}^{R} k_R f(Ts_{x,i}) f(\theta_{x,i}) f(O_{x,i}) dt \quad (14)$$

$$Rg_{x,i} = k_g P_g fr_{x,i} \quad (15)$$

where M^R is the root biomass; k_R is the specific respiration rate of roots; k_g is the fraction of photosynthetic assimilate consumed by growth respiration; $fr_{x,i}$ is the mass fraction of roots in soil layer (*x*, *i*). P_g is the photosynthesis rate of plants. P_g was estimated using a modified Farquahar's leaf biochemical model (see Chen et al., 1999). This model simulates photosynthesis based on biochemical parameters (i.e., the maximum carboxylation velocity, V_{max}, and maximum rate of electron transport, J_{max}), foliage temperature (*Tc*) and stomatal conductance (*gs*). The values of V_{max}

and J_{max} were obtained from in situ measurements from the site (Jia et al., unpublished). *Tc* and *gs* were given in the energy balance sub-model, which was detailed in Gong et al. (2016).

N content bonded in SOM mineralized and was added to soil layers simultaneously with decaying. The abundance of mineral N (i.e. NH_4^+ and NO_3^-) regulates the growth of microbial biomass and r_E following Smith et al. (2010) and Gong et al. (2014). Key processes governing the dynamics of mineral N pools included nitrification-denitrification (Smith et al., 2010), solvent transport with water flows (Gong et al, 2014) and the N uptake by root system. However, the plant growth was not modelled in this work and therefore, N_{upt} was calculated using the steady-state model of Yanai (1994), based on the transpiration rate, surface area of fine roots and the diffusion of solvents from pore space to root surface:

$$N_{upt} = 2\pi r_o L \alpha C_o dt \quad (16)$$

where r_o is the fine root diameter; L is the root length, and $2\pi r_o L$ is the surface area of fine roots; α is the nutrient absorbing power, which denotes the saturation degree of solute uptake system ($\alpha \in [0,1]$); C_o is the concentration of solvents at the root surface, and is a function of bulk concentration of mineral N (N_{min}), inward radial velocity of water at the root surface ($v_o = E/(2\pi r_o L)$) and saturation absorbing power α. Further details for calculations of α and C_o can be found in work of Yanai (1994).

2.2.3 Submodel (iii): CO_2 exchange of biocrust and photodegradation

Biocrusts are vertically layered systems that comprise topcrust (or, bio-rich layer) and underlying subcrust (or, bio-poor layer), which are different in microstructure, microbial communities and C functioning (Garcia-Pichel et al., 2016; Raanan et al., 2016). Topcrust is usually few-millimetre thick, which allows the penetration of light and the development of photosynthetic microbes (Garcia-Pichel et al., 2016). On the other hand, the subcrust has little photosynthetic-activity. We here focused mainly on describing the C exchanges in the topcrust, but assumed the C processes in the subcrust were similar to those in the underneath soil. We developed the following functions to describe the C fixation and mass balance in the topcrust,

$$F_{Ct} = P_{Ct} - R_{Ct} \quad (17)$$

where P_{Ct} is the bulk photosynthesis rate; and R_{Ct} is the bulk respiration rate. P_C and R_C were further modelled as follows:

$$P_{Ct} = \frac{\alpha_C A_{PAR} P_{Cm}}{\alpha_C A_{PAR} + P_{Cm}} \quad (18)$$

$$R_{Ct} = M_{Ct} k_{cr} f_{RC}(T_{Ct}) f_{RC}(\theta_{Ct}) \quad (19)$$

where α_C is the apparent quantum yield, P_{Cm} is the maximal rate of photosynthesis, and was a function of the moisture content (θ_{Ct}) and temperature (T_{Ct}) in topcrust; A_{PAR} is the photosynthetically active radiation (PAR); M_{Ct} is the total C in the SOM of topcrust; k_{cr} is the respiration coefficient; $f(\theta_{Ct})$ and $f(T_{Ct})$ are water and temperature multipliers. Here, we assumed no photosynthesis in subcrust. The heterotrophic respiration (R_{Cs}) was calculated as was done for soil respiration (Eq. (11)) based on the C storages ($M^r_{x,1}$) and temperature and moisture content of crust layer (i.e. $Ts_{x,1}$ and $\theta_{x,1}$; see Eq. (29) and Eq. (14) in Gong et al., 2016).

To consider different C losses and exchanges, and to calculate the C balance in topcrust and subcrust, respectively, we considered the following matters. R_{Ct} includes the respirations from both autotrophic (M_{CA}) and heterotrophic (M_{CH}) pools. When autotrophic organisms die, SOMs pass from M_{CA} to M_{CH} and influence the turnover processes. A variety of topcrust organisms can reach into subcrust (e.g. through rhizines, Aguilar et al., 2009) and export litters there. When the surface is gradually covered by deposits, topcrust organisms tend to move upward and recolonize at the new surface (e.g. Garcia-Pichel and Pringault, 2001; Jia et al., 2008), leaving old materials buried into the subcrust (Felde et al., 2014). On the other hand, the debris left to soil surface are exposed to photodegradation. Based on above, the C balance in topcrust and subcrust was calculated as following, assuming the partitioning of respiration between autotrophic and heterotrophic pools was proportional to their fractions:

$$M_{Ct} = M_{CA} + M_{CH} \tag{20}$$

$$\frac{dM_{CA}}{dt} = P_{Ct} - R_{Ct}\frac{M_{CA}}{M_{Ct}} - k_m M_{CA} - k_b M_{CA} \tag{21}$$

$$\frac{dM_{CH}}{dt} = k_m M_{CA} - R_{Ct}\frac{M_{CH}}{M_{Ct}} - k_b M_{CH} - F_P \tag{22}$$

$$\frac{dM_{Cs}}{dt} = k_b M_{Ct} - R_{Cs} \tag{23}$$

where k_m is the rate of C transfer (e.g. mortality) from autotrophic pool to heterotrophic pool; k_b is the rate of C transfer (e.g. burying) from topcrust to subcrust; F_P is the loss of SOM due to photodegradation.

Photodegradation tends to decrease surface litter masses in a near linear fashion with the time of exposure (Austin and Vivanco 2006; Vanderbilt et al., 2008). Considering the diurnal and seasonal variations of radiation, F_P was calculated as a function of surface SOM mass and solar radiation:

$$F_{P_x} = M_{surf} k_p Rad_x \tag{24}$$

where Rad_x is the incident shortwave radiation at surface x (Gong et al., 2016); M_{surf} is the surface litter mass; and k_p is the photodegradation coefficient.

2.3 Micrometeorological and soil CO_2 efflux measurements

Meteorological variables were measured every 10 seconds and aggregated to half-hourly resolution during 2013-2014. The factors measured included the incoming and outgoing irradiances (PAR-LITE, Kipp and Zonen, the Netherlands), PAR (PAR-LITE, Kipp and Zonen, the Netherlands), air temperature and relative humidity (HMP155A, Vaisala, Finland). Rainfall was measured with a tipping bucket rain gauge (TE525WS, Campbell Scientific Inc., USA) mounted at a nearby site (1 km away, see Wang et al., 2014a). The seasonal trends of the measured *Ta* and *P* can be found in Jia et al. (2016). No surface runoffs were observed at the site, indicating the horizontal redistribution of rainfall was mainly through subsurface flows.

Continuous measurements of F_S were conducted using an automated soil respiration system (model LI-8100A fitted with a LI-8150 multiplexer, LI-COR, Nebraska, USA). The system was on a fixed sand dune of typical size (Wang et al., 2014a), which was located about 1.5 km south from the EC tower described in Gong et al (2016). Three collars (20.3 cm in diameter and 10 cm in height, of which 7 cm inserted into the soil) were installed on average at 3m spacing in March 2012. One collar (C1, see Fig. 1c) was set on a bare soil microsite with no presence of biocrust. Two other chambers (C2, see Fig. 1d and C3, see Fig. 1e) were set on lichen-crusted soils. F_S was measured hourly from C1 and C2 by opaque chambers, whereas by transparent chamber from C3 to include the photosynthesis and photodegradation. Litters from the shrub canopies were cleared from the collars during weekly maintenance. Hourly *Ts* and θ at 10 cm depth were measured outside each chamber using the 8150–203 soil temperature sensor and ECH2O soil moisture sensor (LI-COR, Nebraska, USA), respectively. Root biomass was sampled near each collar (within 0.5 m) in July 2012, using a soil corer (5 cm in diameter) to a depth of 25 cm. The samples were mixed and sieved sequentially through 1, 0.5 and 0.25 mm meshes, and the living roots were picked by hands. The comparison of the three micro-sites is shown in Table 1. Methods used in data processing and quality control have been described earlier in details (see Wang et al., 2014a, 2015). The quality control led to gaps of 10 - 13% in the F_s dataset.

2.4 Model set-ups

2.4.1 Parameterization of vegetation and soil texture

The parameterization schemes supporting the simulations of energy balance and soil hydrology in sub-model (i) - (v) have been described previously in detail by Gong et al. (2016). As the water-energy budget is sensitive to vegetation (i.e. canopy size, density and leaf area) and soil hydraulic properties (see Gong et al., 2016), we hereby revalued these parameters for the F_S site. Measurements based on four 5m×5m plots showed that the crown diameter *D* (86 ± 40 cm) and height *H* (47± 20 cm)

at this site were similar to those measured from the eddy-covariance (EC) footprint by Gong et al. (2016). However, the shrub density was 50% greater, leading to higher shrub coverage (42%), shorter spacing distance L (40.2 cm) and greater foliage area. On the other hand, the subsoil at the F_S site is sandy and much coarser than that at the EC footprint. Therefore, we collected 12 soil cores from 10 cm depth, and measured saturated water content (θ_{sat}), bulk density and residual water content (θ_r) from each sample. Then, the samples were saturated, and covered and drained by gravity. We measured the water content after 2-hour and 24-hour draining, which roughly represented the matrix capillary water content (10 kPa) and field capacity (33 kPa) (Armer, 2011). The shape parameters n and α_h (see Eq. (26) in Gong et al. 2016) for the water-retention function were estimated from these values (Table 2).

2.4.2 Parameterization of soil C and N pools

The sizes and quality of soil C pools were parameterized based on a set of previous studies. The total SOC in the root-zone soil (i.e. 60cm depth, bulk density of 1.6 g cm^{-3}) was set to 1200 g m^{-2}, based on the values reported from previous studies in Yanchi area (e.g. Qi et al., 2002; Chen and Duan, 2009; Zhang and Hou, 2012; Liu et al., 2015; Lai et al., 2016). The mass fraction of resistant SOM pool (M_{hum}) was set to 40 - 50 % of total SOM, following work by Lai et al. (2016). The vertical distribution of the SOM pools was described following Shi et al. (2013). At the ecosystem level, the aboveground biomass was linearly related to the crown projection area ($M^S = 0.2917 * \pi(0.5D)^2$, see Zhang et al., 2008). The total root biomass was then calculated as proportional to the aboveground biomass, using a root-shoot ratio of 0.47 ($M^R = 0.47M^S$, Xiao et al., 2005). The vertical profile of root biomass was parameterized as decreasing exponentially with depth, using the depth profile reported by Lai et al. (2016). On the horizontal direction, root biomass was set to decrease linearly with the distance from the centre of a shrub crown (Zhang et al., 2008). The N content was parameterized following the measurement of Wang et al. (2015).

Based on the above settings, the specific decomposition rate of debris was estimated from the litterbag experiment of Lai et al. (2016), which showed a 16% decrease in the mass of fine-root litters during a 7-month period of year 2013 at the Yanchi site. The photodegradation coefficient (k_p) was set to 0.23 yr^{-1}, which was the mass-loss rate reported by Austin and Vivanco (2006). M_{surf} was set to 33% of M_{CH} in topcrust, assuming the depth of light penetration was about 2 mm and C concentration was homogeneous in topcrust. The surface litter from canopy was not considered in this modelling, as the plant litters were cleaned from the collars during weekly maintenance. The specific respiration rate of roots (k_R), however, could be much greater during vegetative growing stage than other periods, e.g. at the defoliation stage (Fu et al., 2002; Wang et al., 2015). Here we linked k_R to the development of foliage in modelling using the approach of Curiel Yuste et al. (2004):

$$k_R = k_{R0}(1 + n_R L_l / L_{max}) \quad (25)$$

where k_{R0} is the "base" respiration rate (Table 2); L_l is the green leaf area, which is a function of Julian day (Gong et al., 2016); L_{max} is the maximum L_l; n_R is the maximum percentage of variability and is set to 100%.

2.4.3 Parameterization of soil CO_2 production

Based on the empirical study of Wang et al. (2014a), the steady-state sensitivity of CO_2 production to soil temperature and water content (i.e., $f(Ts)f(\theta)$, Eq. (11)) can be described as a logistic-power function:

$$f(Ts)f(\theta) = f(Ts,\theta) = \{1 + \exp[a(b - Ts)]\}^{-1}(\theta/\theta_{sat})^c \quad (26)$$

where a, b and c are empirical parameters. This function represents the long-term water-thermal sensitivity of CO_2 production over the growing seasonal, yielding an apparent temperature sensitivity Q_{10} of 1.5 for the emitted CO_2 (Wang et al. 2014a). However, this could underestimate the short-term sensitivities of CO_2 production. The apparent Q_{10} could be much greater at the diurnal level than at the seasonal level (Wang et al., 2014a). In this work, we firstly calculated the "base" sensitivity using the long-term scheme (Eq. 26) with 1-day moving average of water-thermal conditions. Then the deviation of hourly sensitivity from "base" condition was adjusted by the short-term Q_{10}:

$$f(Ts)f(\theta) = f(Ts_{short},\theta_{short}) + [f(Ts,\theta) - f(Ts_{short},\theta_{short})]Q_{10}^{(Ts-Ts_{short})/10} \quad (27)$$

$$Q_{10} = \max\left[Q_{10}(Ts_{short}), Q_{10}(\theta_{short})\right] \quad (28)$$

$$Q_{10}(Ts_{short}) = -0.42\,Ts_{short} + 12.4 \quad (29)$$

$$Q_{10}(\theta_{short}) = 18010\,\theta_{short}^{3.721} + 1.604 \quad (30)$$

where Ts_{short} and θ_{short} are the 1-day moving averages of Ts and θ, respectively; Q_{10} (Ts) and Q_{10} (θ) are the adjustment functions for short-term apparent Q_{10}, regarding the short-term Ts and θ.

Further non-linearity of soil respiration responses refers to the rain-pulse effect (or the "Birch effect", Jarvis et al. 2007), that respiration pulses triggered by rewetting can be orders-of-magnitude greater than the value before rain event (Xu et al., 2004; Sponseller, 2007). Such response could be very rapid (e.g. within 1 hour to 1 day, Rey et al. 2005) and sensitive to even minor rainfalls. It also seems that the size and duration of a respiration pulse not only depend on the precipitation size, but also on the moisture conditions prior to the rainfall (Xu et al., 2004; Rey et al., 2005; Evans and Wallenstein, 2011). As numerical descriptions on such an effect remain unavailable at the moment, we simply multiplied Eq. (26) to a rain-pulse coefficient (f_{pulse}):

$$f_{pulse} = max[1, (\theta/\theta_{72h})^{n_p}] \quad (31)$$

where is the 3-day moving average of soil moisture content; n_p is a shape parameter and was set to 2 in this study. θ_{72h} is the 72-hour moving average of θ. For tests on model sensitivities to different parameterization of f_{pulse} see section 2.5.3.

2.4.4 Parameterization of biocrust photosynthesis and respiration

In sub-model (iii), Equations (17) - (19) were parameterized based on the experiment of Feng et al. (2014). In the experiment, 50 lichen (topcrust) samples of 0.5-0.7 cm thickness (100% coverage, average C content of 1048 umol C cm^{-3}) were collected from a 20 m × 20 m area. The samples were wetted and incubated under controlled T_{Ct} (i.e. 35°C, 27°C, 20°C, 15°C, and 10°C). These samples were divided into two groups to measure the net primary productivity (NPP) and dark respiration (Rd) separately. Gas exchanges and light response curve for each crust sample were measured using LI-6400 infrared gas analyzer equipped with an LI-6400-17 chamber and an LI-6400-18 light source (LI-COR, Lincoln, NE, USA). Measurements were taken at ambient CO_2 values of 385 ± 35 ppm. Saturated topcrust samples were placed in a round tray and moved to the chamber. CO_2 exchange was measured during the drying of samples, until the CO_2 flux diminished. During drying, θ_{Ct} was measured every 20 min. For more details see Feng et al. (2014).

Fitting measured Rd to T_{Ct} and θ_{Ct} (see Fig. 3a) using Matlab® (2012a) curve-fitting tool. The obtained multipliers in Eq. (19) are as following:

$$f_{RC}(T_{Ct})f_{RC}(\theta_{Ct}) = Q_{Ct}^{\frac{(T_{Ct}-20)}{10}}(a_{RC} + b_{RC}\theta_{Ct} + c_{RC}\,\theta_{Ct}^{2}) \quad (32)$$

where Q_{Ct}, a_{RC}, b_{RC}, c_{RC} are the fitted shape parameters (Table 2).

The parameterized Eq. (19) was then used to simulate the Rd for the NPP samples, based on the correspondent T_{Ct} and θ_{Ct} of each measurement. P_{Cm} was determined by subtracting the simulated respiration rate from the NPP measured under light-saturated conditions. Then P_{Cm} was fitted to T_{Ct} and θ_{Ct} in Matlab® (2012a) curve-fitting tool using following equation (Fig. 3b):

$$P_{Cm} = f_{Pt}(T_{Ct})\, f_{Pw}(\theta_{Ct})$$

$$= \left(a_{Pt} + b_{Pt}T_{Ct} + c_{Pt}\,T_{Ct}^{2} + d_{Pt}\,T_{Ct}^{3}\right)\left(-a_{Pw} + b_{Pw}\theta_{Ct} - c_{Pw}\,\theta_{Ct}^{2} + d_{Pw}\,T_{Ct}^{3}\right) \quad (33)$$

where a_{Pt}, b_{Pt}, c_{Pt}, d_{Pt}, a_{Pw}, b_{Pw}, c_{Pw}, d_{Pw} are fitted shape parameters (Table 2).

It should be addressed that T_{Ct} and θ_{Ct} could change more rapidly than the mean conditions of the crust (i.e. $Ts_{x,1}$ and $\theta_{x,1}$). In this work, T_{Ct} was calculated from the surface temperature (T_x, see Eq. (13) in Gong et al., 2016) and $Ts_{x,1}$ by linear interpolation. The calculation of θ_{Ct}, on the other hand, depended on the drying-rewetting cycle. During drying phases, θ_{Ct} was interpolated linearly from $\theta_{x,1}$

and surface moisture content (θ_x); whereas during wetting phases, the mass balance of water input P and evaporation loss ($E^s_{x,1}$, see Eq. (17) in Gong et al., 2016) was considered:

$$T_{Ct} = \frac{T_x Z_{Ct} + Ts_{x,1} Zs_{x,1}}{Z_{Ct} + Zs_{x,1}} \quad (34)$$

$$\theta_{Ct} = max\left[\frac{\theta_x Z_{Ct} + \theta_{x,1} Zs_{x,1}}{Z_{Ct} + Zs_{x,1}}, \theta_{Ct} + \frac{P - E^s_{x,1}}{Z_{Ct}}\right] \quad (35)$$

where $Zs_{x,1}$ is the thickness of the biocrust; and Z_{Ct} is the thickness of the topcrust. θ_x was calculated from the surface humidity and the water retention of the crust layer, using Eq. (25) – (26) by Gong et al. (2016).

2.4.5 Calculation of litter input to soil and SOC transport in biocrust

The litterfall added to each soil layer ($A^1_{x,i}$, Eq. (13)) were linked to the mortality of roots, which was calculated following Asaeda and Karunaratne (2000).

$$A^1_{x,i} = k_{mo} Q_{mo}{}^{Ts_{x,i} - 20} M^R_{x,i} \quad (36)$$

where k_{mo} is the optimal mortality rate at 20ºC; Q_{mo} is the temperature sensitivity parameter (Asaeda and Karunaratne, 2000). Similarly, we attributed the C transport rate (A_{Cm}) from M_{CA} to M_{CH} mainly to the mortality of autotrophic organisms. We assumed that most mortality of crust organisms occurred during abrupt changes in wetness, as microbial communities may adapt slow moisture changes or remain inactive during drought (e.g. Roberson and Firestone, 1992; Reed et al., 2012; Coe et al., 2012; Garcia-Pichel et al., 2013; Maestre et al., 2013). Here, we introduced a water-content multiplier, $f_m(\theta_{Ct})$, to describe the impact of abrupt θ_{Ct} changes on k_m:

$$A_{Cm} = k_{mc} Q_{mo}{}^{T_{Ct} - 20} f_m(\theta_{Ct}) M_{CA} \quad (37)$$

$$f_m(\theta_{Ct}) = \max[0.01, 1 - \min(\theta_{Ct}, \theta_{Ct7}) / \max(\theta_{Ct}, \theta_{Ct7})] \quad (38)$$

where k_{mc} is the optimal mortality rate at 20ºC; Q_{mo} is the temperature sensitivity parameter (Asaeda and Karunaratne, 2000); θ_{Ct7} is the forward 7-day moving average of θ_{Ct}.

C transport from topcrust to subcrust was calculated as driven mainly by the sand deposition and burying of topcrust SOM. Assuming the C content in topcrust was homogeneous and the thickness Z_{Ct} was near-constant, the transport rate (k_b) was then proportional to the sand deposition rate:

$$k_b = \frac{k_{sand}}{\rho_{bulk}} \frac{1}{Z_{Ct}} \quad (39)$$

where ρ_{bulk} is the bulk density of soil; k_{sand} is the sand deposition rate in Yanchi area, which is a function of wind velocity (Li and Shirato, 2003):

2.5 Model validation and sensitivity analyses

2.5.1 Simulation set-ups

In the model simulations, soil depth was set to 67.5 cm to cover the rooting zone (Gong et al., 2016), including the crust layer (2.5 cm) and sandy subsoil (65 cm, stratified into 5 cm layers). Water content measured at 70 cm depth was used as the lower boundary condition for hydrological simulation (Jia et al., 2014). The calculation of soil temperature extended to 170 cm depth with no-flow boundary, regarding the probably strong heat exchange at the lower boundary of rooting zone (Gong et al., 2016). Zero-flow condition was set for the lower boundary of CO_2 and O_2 gases, whereas dissolved CO_2 was able to leech with seepage water. Based on presumed similarity of RLU structures, we assumed no-flux conditions for transports of water, heat, solvents and gases at outer boundary. In the simulation, we assumed instant gas transport via topcrust, whereas considered the CO_2 released by subcrust (R_{Cs}) was subject to the dissolving-transport processes. In this work, we aggregated the C processes in subcrust with those in soil profile. The initial ratio of M_{CA} : M_{CH} was set to 2:3. The C concentration of organic matters was set to 50%.

The model run with half-hourly meteorological variables including the incoming shortwave radiation, incoming longwave radiation, PAR, *Ta*, relative humidity, wind speed and precipitation. Initial temperatures and soil moisture content for each soil layer were initialized following the work by Gong et al. (2016). Surface CO_2 concentration was set to 400 ppm. The initial gaseous CO_2 concentration was set to increase linearly with depth (5 ppm cm^{-1}). The initial CO_2 concentration in liquid form was then calculated based on Eq. (4) – Eq. (8). The initial content of mineral N content was set to 40 mg/g, which was within the range of the field observations. The two-dimensional transpirations of water, energy and gases along the soil profile were solved numerically using the Predict–Evaluate–Correct–Evaluate (PECE) method (Butcher, 2003). In order to avoid undesired numerical oscillations, the transport of water, energy and gases were calculated at 5-min sub steps.

2.5.2 Model validation

First, we validated the modelling of soil temperature and moisture content for the F_S site (Test 0). The simulated hourly soil temperature and moisture content at 10 cm depth were compared to the measured values for each collar. The validation was based on the same meteorological data as used by Gong et al. (2016), who validated the model in regard to the diurnal to seasonal dynamics of radiation balance, surface energy balance, soil temperature and moisture content at the EC site.

The validity of the modelled F_S was then examined in three separate tests. In Test 1, modelled F_S was validated for non-crusted soils. In this case, F_T in Eq. (1) was the only term affecting F_S (F_B=0 and F_P = 0), and the crust influences on C-water exchanges were excluded. The biocrust-

494 relatedprocesses were considered in Test 2 and Test 3. Test 2 considered the dark respiration of
495 biocrust (R_{Ct}), and set $F_B = R_{Ct}$ and $F_P = 0$. Test 3 considered all the flux components (F_T, F_P and F_B).
496 In these tests, different values of root biomass were assigned to the model regarding the different
497 collar conditions (Table 1). In Test 1 – Test 3, half-hourly F_S were simulated and averaged to hourly
498 values, and compared to the those measured from the collar C1 – C3, respectively. Linear regressions
499 were used to compare the modelled and measured values. The biases (ζ) of the simulated values were
500 calculated by subtracting the measured values from the modelled ones. Gap values in the
501 measurements were omitted in the validation and the bias analyses.

502

503 **2.5.3 Simulating componential CO_2 fluxes and their parameter sensitivities**

504 Using the validated model, we simulated the temporal trends of C flux components (i.e. P_{Ct}, R_{Ct}, F_P,
505 F_T, *Ra* and *Rs*) in Test 4, in order to find out how the different flux components may have contributed
506 to the total efflux (Table 3). The simulation used the same model set-ups and climatic variables as
507 Test 3. It should be noticed that, although the model was built as an abstract for ecosystem-level
508 processes, the simulation set-ups and validation were performed at a point level corresponding to
509 respiration chambers. Therefore, understanding the uncertainty sourced from parameterization could
510 be helpful for future development and applications. In Gong et al. (2016), we have studied the
511 sensitivities of modelled soil temperature and moisture content to the variations in soil texture, water
512 retention properties, vegetation parameters and plant-interspace heterogeneities. In this study, we also
513 tested the sensitivity of F_S and componential fluxes to the changes in a number of site-specific
514 parameters (Table 4). These parameters included pH, nitrogen content, water-thermal conditions, root
515 biomass, production and decomposability of litters, which are often key factors regulating soil C
516 processes but likely to vary within and among ecosystems (see e.g. Ma et al., 2011; Gong et al., 2016;
517 Wang et al., 2016). Furthermore, we tested the model sensitivities to several newly defined
518 parameters (i.e. n_R, n_p and f_m), to understand their effects on model uncertainties. F_S and componential
519 fluxes at interspace were simulated by varying single parameter value by 10% or 20%. The sensitivity
520 of each tested flux was described by the difference (dF) in the annual flux rate simulated using
521 manipulated parameter, as compared to the rate simulated under no-change conditions.

522

523 **2.5.4 Comparing model sensitivities between plant cover and interspace**

524 In order to study the effects of plant-interspace heterogeneity on soil CO_2 efflux, Test 5 simulated
525 annual F_S and componential fluxes at plant cover and compared the values to interspace. The
526 simulation set-ups were almost same as those employed in Test 1-3; only exception was that same
527 initial values of SOC storages (650 gC m-2) and root biomass (200 g m-2) were used for under-
528 canopy and interspace areas for comparison purpose. Based on Test 4, we further compared the plant-
529 interspace differences in the C-flux sensitivities to most important site-specific parameters, i.e. soil

temperature (*Ts*), water content (θ) and root biomass (M^R) (see Section 3.2). The differences in parameter sensitivities were calculated by comparing the absolute values of sensitivities ($|dF|$, see section 2.5.3 and Table 4) from the area with plant cover to without (interspace).

3. Results

3.1 Model validity

Comparing to the EC site in previous work (Gong et al., 2016), the soil in this study is much coarser and the measured θ at 10 cm depth was constantly lower (Fig. 4), indicating the necessity of re-parameterization and validation of the water-energy algorithms. Figure 4a shows the modelled hourly *Ts* and θ at 10 cm depth with the mean values measured from the F_S site during year 2013. Based on the site-specific vegetation and soil texture parameters, our model explained 97% of the variations in the measured hourly *Ts*. The model underestimated the temperature mainly in summer time (i.e. day 150-250, Fig. 4a). The underestimation was more pronounced around the noontime in the diurnal cycle. As the water-content sensors may not accurately capture the moisture dynamics during freezing period, only the simulation during ice-free period were compared to measured data (Fig. 4b). During the ice-free period, the model explained 83% of the variations in the measured mean water contents at 10 cm depth. The biases in the modelled temperature and moisture content were less than the spatial variations observed in this area (e.g. Wang et al., 2015). Therefore, our model could be able to reproduce the time series for the measured water-energy fluxes at the site.

Our modelling reasonably reproduced the diurnal and seasonal fluctuations of F_S. The model explained 87 and 83% of the variations in the hourly F_S measured on the non-crusted surface in year 2013 and 2014 (Fig. 5a). The root-mean-square errors (RMSE) were 0.43 umol m^{-2} s^{-1} and 0.29 umol m^{-2} s^{-1} respectively. The model mainly underestimated the daytime F_S during the freezing seasons. During the ice-free periods, the model maily overestimated the efflux in early springs. The biases in modelling largely showed a diurnal pattern (Fig. 5b), that F_S was mainly underestimated in noon hours (i.e. from 10 a.m. to 3 p.m.) but slightly overestimated in the afternoon and evening. At the daily level, our model explained 94% of the variations in measured daily efflux during the two-year period (Fig. 5c).

Compared to the non-crusted soil (C1), the simulated F_S for crusted surfaces (C2 and C3) showed greater deviations from measured data. At the hourly scale, our model explained 75 % (year 2013) and 68 % (year 2014) of variations in measured F_S from C2 (Fig. 6a), and 68 % (year 2013) and 61 % (year 2014) of variations in measured F_S from C3 (Fig. 6b). For the two-year period, RMSE of the modelled hourly F_S were 0.25 umol m^{-2} s^{-1} and 0.35 umol m^{-2} s^{-1} for C2 and C3, respectively. The magnitudes of biases ($|\zeta|$) were generally greater during the rainfall period (i.e. from the start of raining to 24 hours after end of rainfall) than the inter-rainfall period (Fig. 7). The simulated F_S for C2 showed similar diurnal pattern of biases as compared to C1, suggesting ineligible contributions of

biases in the simulated subsoil emissions. Introducing photosynthesis and photodegradation of biocrust to the system (C3) led to greater overestimations in F_S, and this was more obvious in the afternoon hours (i.e. from 12 a.m. to 6 p.m.) and during wetting period. Nevertheless, at the daily scale, the model explained 91% (C2, Fig. 5c) and 86% (C3, Fig. 5d) of the variations in the measured F_S during the two-year period. There were no significant systematic deviations between the measured and the modelled daily values, as indicated by regression slopes close to 1 and intercepts close to 0 (Figs. 4 and 5).

The results above showed that, the model well described the seasonal variations of F_S for both non-crusted and lichen-crusted soils. Moreover, the model was able to capture the strong variability of hourly/daily F_S in wetting-drying cycles. Comparing to earlier statistic modelling by Wang et al. (2014a, 2014b), this model showed equality or improvement in performance. In this sense, we assume that our model has included the main mechanisms controlling the F_S dynamics in the soil system, and could be used for further analysis on componential C processes and their parameter sensitivities.

3.2 Modelled C flux components of F_S

Test 4 showed that, *Rs* was the main contributor to the root-zone CO_2 production, which accounted for a major source of effluxes (F_S). Our measurements showed large diurnal and seasonal variations in F_S regardless the existence of crust covers (Fig. 5 and Fig. 6). Particularly, the F_S dynamics depended strongly on rain events. Even at non-crusted soil (i.e. C1), F_S dropped significantly from the pre-rainfall level even to near-zero, but rebound rapidly and peaked after rain stopped (Fig. 5a). This could relate to the mismatched trends of CO_2 production (*Rs* + *Ra*) and emission (F_T) from the rooting zone with respect to the wetting-drying cycles (Fig. 8a). Compared to CO_2 production, the responses of F_T to rainfall were generally lagged and smoothed (see examples in Fig. 8b – 8d), irrespective of the size of rain events. In the simulation, soil rewetting increased CO_2 production rapidly but depressed F_T, which increased after rain ceased. In all the examples (Fig. 8b – 8d), F_T exceeded R_P within 48 hours after the ending of rain events. At the annual level, the total R_P was larger during wetting period (i.e. raining days plus 1 day after rainfall) than the rest days of the year (i.e. drying period), whereas the total F_T was greater during the drying period (Fig. 8e).

On the annual basis, CO_2 production (*Rs*+*Ra*) and emission (F_T) from root-zone soil were mismatched (Table 3), and the former was more than 15 % greater than latter. Such a gap was mainly due to the root uptake and transport of dissolved CO_2 (i.e. 36 gC m^{-2} $year^{-1}$), whereas the loss of dissolved CO_2 via seepages or pore-mediated horizontal flows were limited (i.e. 7.4 gC m^{-2} $year^{-1}$). The photosynthesis rate of topcrust was 31.1 gC m^{-2} $year^{-1}$ at interspace. After rainfall, the C uptake by topcrust increased significantly, even turned the soil from net C source to sink during a few hours to one day (Fig. 6, Fig. 8). However, at annual scale, the C losses via respiration and photodegradation

accounted for 90 % of the photosynthetic products, leading to a near-zero contribution of topcrust to F_S during the two year period (i.e. < 5 gC m^{-2} $year^{-1}$).

Analysis of parameter sensitivity showed that, the modelled F_S and the component fluxes were more sensitive to ± 2 ºC in *Ts* or ±10 % in θ, compared to the effects of ±10 % or ±20 % in the other parameters (Table 4). Varying θ by 10 % produced greater impacts on the simulated R_P and crust-related fluxes (i.e. P_{Ct}, R_{Ct} and F_P), as compared to changing *Ts* by ± 2 ºC. Increasing θ by 10 % enhanced the simulated P_{Ct} and F_{Ct} by 41 % and 28 %, and doubled the net C sequestration ($F_{Ct} - F_P$) by topcrust. However, the contribution of such changes to annual F_S was minor, and amounted for only 2.0 % of the total efflux. Beside *Ts* and θ, the simulated efflux was also sensitive to changes in root biomass (M^R). Manipulating root biomass by ±10 % changed the annual F_T and F_S by about 7%, and such effects were 100% greater than ±10 % changes in M_{tot} in soil. Adjustment of other parameters, e.g. n_p (eq. (31)) and f_m (eq. (38)), produced little influences on the modelled F_S and the componential fluxes (Table 4). In addition, the model was robust to the adjustment of several crust-related parameters, i.e. k_{mc}, M_{Ct} and M_{CA}: M_{CH}. Hence, algorithms correspondent to those parameters could be simplified in future developments.

3.3 Modelled plant-interspace differences in C flux components

At either plant-covered or interspace area, *Rs* was a major contributor to root-zone CO_2 produced and F_T dominated the total effluxes (Table 3). The C loss at interspace was 14% faster than under-canopy on an annual basis, if root biomass and SOC were homogeneous at plant cover and interspace. The lower F_S rate at plant cover mainly attribute to the lower CO_2 production (R_S+R_a) from subsoil. The C loss via seepage and root transport, which is the gap between subsoil CO_2 production and emission (F_T), was slightly higher under canopy (17%) than at interspace (15%). Comparing to interspace, the photosynthesis of biocrust (P_{Ct}) was 34% lower under canopy. This reduced the under-canopy F_{Ct} by 42% in comparison with interspace. However, such a different was largely offset by the reduced photodegradation rate under canopy, leading to limited differences in net sequestration of topcrust between plant-interspace (i.e. by 1.4 gC m^{-2} $year^{-1}$).

We further compared the flux sensitivities at plant cover and interspace to the changes in three most effective parameters (i.e. *Ts*, θ and M^R, see Table 5). For subsoil-mediated fluxes (i.e. F_S, F_T, R_a, R_S), the sensitivity values differed by less than 2 % from plant cover to interspace. On the other hand, the sensitivities of crust-related fluxes (i.e. P_{Ct}, F_{Ct}, F_P) showed greater differences between plant cover and interspace. Comparing to interspace, F_S and F_T at plant-covered area were more sensitive to *Ts* changes, but less sensitive to manipulations in θ. On the other hand, the plant cover reduced the sensitivity of CO_2 effluxes to changes in root biomass. P_{Ct}, F_{Ct} and F_P were generally more sensitive to warming and θ manipulations at plant cover than interspace, except that plant cover decreased the

sensitivity of F_P to -10 % changes in θ. Nevertheless, their contribution to the sensitivity of F_S was marginal, due to the low flux rates of crusts.

4. Discussions

4.1 The roles of componential C processes in regulating soil CO_2 efflux

Our process-based model provided a useful tool to separate the multiple soil C processes and investigate their roles in regulating F_S dynamics in dryland ecosystems. So far, efforts to quantify the soil C loss in terrestrial ecosystems have considered soil C efflux as a synonym of respired CO_2. However, based on this work, cautions must be taken when extrapolating the F_S responses from the chamber to ecosystem scale and from short-term to long-term periods. Processes other than autotrophic and heterotrophic respiration could significantly modify the F_S responses to climatic variability. Our simulation highlighted decoupled CO_2 production and emission during the wetting-drying cycle, as regulated by the CO_2 transport in soil profile. The simulated CO_2 production in soil profile were much greater than effluxes during rain pulses (e.g. Fig. 7). This indicated that, the low F_S during rewetting was mainly due to the increase in CO_2 dissolution, instead of the reduced respiration rates by low O_2 supply (e.g. Fang and Moncrieff, 1999). This finding is further supported by the measurement of Maier et al. (2011), which showed that 40% of the respired CO_2 could be stored temporally in soil pore-space after rainfalls. The dissolved CO_2 then released gradually with the evaporation of pore water, leading to lagged responses of efflux as compared to respirations. Regarding that a major fraction of CO_2 was produced during the wetting periods (Fig. 5e), such a lagging effect should be carefully examined when analysing the climatic sensitivity of F_S. Our simulations showed that a considerable fraction of CO_2 produced could be removed by root uptake and leave the volume measured by the respiration chamber. Bloemen et al. (2016) showed that the CO_2 concentration in root xylems could be higher than in soil solutions. This implies that such a "missing source" might be even greater than the model estimation, although knowledge is still limited about the efficiency of the removal and the diffusion/release of CO_2 during the transport (Bloemen et al., 2016).

The contributions of biocrusts as C sink or source have remained largely unknown (Castillo-Monroy et al., 2011). This is mainly due to the difficulty to separate the CO_2 exchanges of crust organisms from the background respirations (Castillo-Monroy et al., 2011; Sancho et al., 2016). As demonstrated in our work (Fig. 5b – 5d), the photosynthesis of topcrust could be masked by background emission quickly (e.g. within 1 day) after rain events. The simulated F_{Ct} was 31 g C m^{-2} $year^{-1}$ at interspace. Considering a 30% coverage of lichens over the sampling area (Feng et al., 2014), the interspace-level NPP was 9.3 g C m^{-2} $year^{-1}$. This value was largely greater than the lab-based estimation for the site (Feng et al., 2014). However, it was in range of the values reported from several other dryland ecosystems (i.e. 5.3 - 29 g C m^{-2} $year^{-1}$, Sancho et al., 2016). Our simulations

672 also suggested that photodegradation might offset about 48 % of the CO_2 photosynthesized by
673 biocrust. It could explain the much higher F_S measured from the transparent chamber (C3) than the
674 opaque chamber (C2) during dry daytime periods (e.g. Fig. 9). It should be also noticed that the litter
675 from shrub canopy was not included in the measurement nor modelling. Also the interactions between
676 photodegradation and biotic decaying were not considered either. Hence, the contribution of
677 photodegradation to soil C balance could be greater than our estimation at the ecosystem level (see e.g.
678 Gliksman et al., 2016). Although the contribution of surface exchanges were only marginal as
679 compared to the annual CO_2 efflux, removing the biocrust processes would significantly reduce the
680 model validity. For example, the goodness of fitting (i.e. R^2) in Test 3 dropped from 0.65 to 0.45 for
681 the two-year period, if F_{Ct} and F_P were neglected. Therefore, delineating the gas exchange of biocrust
682 could be helpful, in order to upscale the modelling of C balance from chamber to ecosystem level,
683 where the distribution of crust cover may vary from one site to another.

684

685 **4.2 Plant-interspace differences in soil C fluxes**

686 Clumped distributions of foliage and biomass are critical features for the adaptation and functioning
687 of vegetation in arid and semiarid environments. Previous studies have mainly emphasized the shrub
688 effects on ecohydrology (e.g. Rongo et al., 2006; Gong et al., 2016) and enrichment of sediments and
689 nutrient, known as "resource island" effects (Reynolds et al., 1999; Rietkerk et al., 2004). Our
690 simulations showed that the presence of shrub canopy also influenced the soil C exchanges. The
691 presence of shrub cover affected the C functioning of biocrust mainly through shading, which reduced
692 photosynthesis more than respiration and photodegradation. Comparing to the interspace, simulated
693 annual F_S was 13% lower under the canopy (Test 5). As we ruled out the plant-interspace differences
694 in SOC and root biomass and the C-flux differences contributed by biocrusts were limited, such a
695 decrease in plant-cover F_S was probably due to the cooling effect of canopy (Gong et al., 2016). This
696 effect was close to the modelled responses of F_S to ± 2 ºC in soil temperature or ± 10% in soil water
697 content. As the density of roots and litter production are commonly larger under canopy than
698 interspace (e.g. Zhang et al., 2008), the lower respiration rate under canopy tends to facilitate the
699 accumulation of biomass and organic matters and feedback to functioning of "resource islands"
700 during prolonged periods.

701 Our simulation further indicated considerable differences in the C-flux sensitivities between areas
702 with plant cover and without. As the C processes and initial conditions were set to be homogeneous,
703 those differences could mainly result from the different water-thermal conditions at plant cover and
704 interspace. For example, the higher temperature sensitivities of F_T, F_S and F_{Ct} may relate to the
705 cooling effect of canopy (see Gong et al., 2016), which may lead to a greater Q10 value for respiration
706 estimations (i.e. eq. (27)). Moreover, the slower decomposition in under-canopy soil could also lead to
707 the lower sensitivities of F_T and F_S to changes in root biomass and SOM contents. On the other hand,

water advection from interspace to plant cover, which may support over 30% of water loss from under-canopy soils (Gong et al., 2016), could help to lower the F_S sensitivity to water content changes at plant cover. The increased water-thermal sensitivities of C exchanges of biocrust could be explained by the less-stressful environment for curst organisms, e.g. higher moisture content but lower radiation and temperature, although the photosynthesis of lichens (P_{Cl}) could be reduced by shading (Table 3). Such heterogeneity of C-flux sensitivities thus should be considered in future studies on the ecosystem-level responses to climate change and extreme climatic events.

4.3 Modelling uncertainties and future research needs

Our model showed its ability to describe the dynamics of soil temperature, moisture content and C effluxes measured for the studied semiarid ecosystem. The uncertainties in the modelling, however, may exist in several aspects. *Firstly*, the representative land unit (RLU) was a statistical simplification to the target ecosystem at footprint scale (Gong et al., 2016), and may not fully capture the spatially explicitly of soil environment and biogeochemistry at ecosystem scale. For example, the model assumed Poisson probability of mutual shading (Bégué et al., 1994), and the probability of shading increased continuously with solar zenith (Gong et al., 2016). However, for explicit space-time, shading is binary. This possibly explains the biases in the estimated net radiation (Gong et al., 2016) and collar temperature around midday, which sequentially affected the simulated F_S (see Fig. 3b). Moreover, field observations showed considerable spatial variations of soil temperature, water content and biogeochemistry (e.g. pH, litter quality and root biomass) within a distance of 3-5 meters. Such variations could well exceed a magnitude of 10 %, and even over 100 % (e.g. Zhang et al., 2008; Feng et al., 2013; Wang et al., 2015). Therefore, the variation of F_S driven by the spatiality of soil factors could be greater than the responses to ±2 °C in soil temperature or ±10 % in soil water content. Therefore, future modelling may need to consider spatially explicit settings, in order to further minimize the gaps between model settings and the reality.

Secondly, the high sensitivity of simulated F_S to soil pH indicated that the uncertainties in inorganic C processes could strongly affect the accuracy of modelling. Our modelling of CO_2 transport was based on gaseous and liquid phases, whereas the solid phase was not involved, despite the high lime content (2300–5400 kg ha^{-1}) in the soil (Feng et al., 2013; Wang et al., 2015). Based on soil samples of similar lime content (2700 kg ha^{-1}), Buysee et al. (2013) showed that neglecting the inorganic C exchanges by solids may underestimate F_S during the heating phase of a day, but overestimate F_S during the cooling phase. This is very similar to the diurnal pattern of biases in our modelling (Fig. 3d). Therefore, further improvement on the modelling may need to consider the solid phase as well.

Thirdly, the current model still lacked mechanistic descriptions on growths of plant and soil microbes. Comparing to many other ecosystems, drylands often feature high root-shoot ratio (Jackson et al., 1996) but low SOC storages. Changes in plant physiology and growth can readily influence root

744 metabolisms and labile SOC pools, hence modify F_S dynamics (Wang et al., 2015). On the other hand,
745 large fluctuation of diurnal and seasonal temperature may drive the microbial communities to shift
746 between warm-adapted to cold-adapted (Van Gestel et al., 2013), which could largely change soil
747 respiration and its sensitivity to freeze-thaw cycles (Van Gestel et al., 2013; Liu et al., 2016). Both the
748 biotic controls are mixed with the legacy effects of climatic variability over annual and inter-annual
749 courses (Sala et al., 2012; Jia et al., 2016; Shen et al., 2016), and could affect the C-water simulations
750 cumulatively through the feedbacks between biomass accumulation and soil biogeochemistry
751 (Bradford et al., 2016). This may explain the decreasing trend of model validity from year 2013 to
752 2014 (Fig. 3, Fig. 4). Therefore, the dynamics of plants and microbial communities are required in
753 future modelling, in order to improve the F_S simulations regarding inter-annual and long-term periods.

754 *In addition*, proper field data are still needed to support the future modelling work. The dataset used
755 in our model validation mainly separated the influences of biocrusts from subsoil respirations.
756 However, some processes like photodegradation and lateral CO_2 transport by root or water flows still
757 require more support from observation. Also, respiration data from shrub-covered soil remains
758 unavailable, as the settlement of soil collars and respiration chambers under canopy could easily
759 interrupt the biophysiology of shrubs. The C functioning of crust organisms is especially sensitive to
760 water content (Table 4). However, track the water content in the very thin layer of topcrust can be
761 very challenging using hour-based meteorological data. Nocturnal water inputs (e.g. dewfalls) are
762 important to the metabolisms of crust organisms (e.g. Liu et al., 2006), but they are hard to be
763 quantified precisely by EC measurement, or models derived from EC data. Moreover, we presumed
764 structural homogeneity for the crust layer and employed constant regime for crust processes. In reality,
765 there may not be clear boundaries between topcrust and subcrust, and even topcrust itself may contain
766 significant variations in microstructure and communities even within one centimetre (Williams et al.,
767 2012; Raanan et al., 2016). The C sequestration of biocrust can be strongly modified by microbial
768 communities directly (Belnap, 2003; Pointing and Belnap, 2012; Feng et al., 2014; Maestre et al.,
769 2015) and through other factors e.g. surface albedo (Chamizo et al., 2012), dew falls (Liu et al., 2006),
770 soil pore forming (Williams et al., 2012; Felde et al., 2014). So far, many questions remain
771 unanswered about the mechanisms that control the colonization, adaption and succession of microbial
772 communities and the structure-function of biocrust (Pointing and Belnap, 2012). Further knowledge
773 on these mechanisms will be helpful to improve the modelling of crust C functioning in response to
774 climate change and extreme climatic events.

775

776

777 **5. Conclusions**

778 This work represents a first attempt to integrate the CO_2 production, transport and surface
779 exchanges (e.g. biocrust photosynthesis, respiration and photodegradation) in F_S modelling for

dryland ecosystems with high plant-interspace heterogeneities. Our model simulated reasonably well the F_S dynamics measured from non-crusted and lichen-crusted soil collars during year 2013-2014, although introducing the gas exchanges of lichen crust decreased the model performance at the hourly scale. However, further model development may still be required on several aspects, e.g. by including: i) the spatial-explicit schemes for surface conditions and soil biogeochemistry; ii) influences of lime and solids on CO_2 transport; iii) growth dynamics of plants; iv) high-resolution dynamics of surface water-thermal conditions and v) the dynamics of microstructure and microbial communities of biocrusts.

Our model simulations highlighted that, the transport processes of inorganic C and the metabolisms of biocrusts could strongly modify the CO_2 efflux, and these influences are closely linked to soil hydrology. Soil rewetting could enhance CO_2 dissolution and delay the emission of CO_2 produced from root-zone. In addition, an ineligible fraction of respired CO_2 could be removed via lateral flows and root uptake, and become "missing" from volumes under respiration chambers. The lichen-crusted soil could temporally shift from net CO_2 source to sink during rewetting, as driven by the photosynthesis of lichens and the restrained CO_2 emissions from subsoil. Whereas after rain events, the CO_2 exchanges of lichens could be easily masked by background emissions from subsoil. Based on our modelling, the annual NPP was 9.3 gC m^{-2} by topcrust at interspace. However, the net C sequestration by topcrust could be marginal, if the photodegradation is accounted. Our modelling further showed different componential C fluxes and sensitivities between plant-covered soil and interspace. The presence of plant cover tended to decrease the root-zone CO_2 production and biocrust C sequestration, but increase the temperature sensitivities of these fluxes. On the other hand, the sensitivities of root-zone emissions to water content was decreased by canopy. This may be due to the advection water flows from the interspace. To conclude, the complexity and plant-interspace heterogeneities of soil C processes should be carefully considered to extrapolate findings from chamber to ecosystem scales, and to predict the ecosystem responses to climate change and extreme climatic events. Our model can serve as a useful tool to simulate the soil CO_2 efflux dynamics in dryland ecosystems.

Acknowledgement

This modelling work was carried out under the Finnish-Chinese research collaboration project EXTREME (2013-2016) by the University of Eastern Finland and Beijing Forestry University. The instrumentation and field measurements utilized in this work were supported by National Natural Science Foundation of China (NSFC) (Proj. No. 31361130340, No. 31670710 and 31670708) and Beijing Forestry University. The modelling work of EXTREME project was supported by the Academy of Finland (proj. no. 14921) and the University of Eastern Finland. Thanks to Peng Liu,

Huishu Shi, Yuming Zhang, Sijing Li, Zhihao Chen, Siling Tang, Yajuan Wu and Yuan Li for assistance on the field measurements and instrumentation maintenance.

References

Asaeda, T., Karunaratne, S., 2000. Dynamic modeling of the growth of Phragmites australis: Model description. Aquatic Botany 67, 301–318.

Aguilar, A.J., Huber-Sannwald, E., Belnap, J., Smart, D.R., Moreno, J.T.A., 2009. Biological soil crusts exhibit a dynamic response to seasonal rain and release from grazing with implications for soil stability. Journal of Arid Environment 73, 1158–1169.

Armer, A.M., 2011. Prediction of hydraulic conductivity and sorptivity in soils at steady-state infiltration. Archives of Agronomy and Soil Science 58, doi:10.1080/03650340.2011.572877

Austin, A.T., Vivanco, L., 2006. Plant litter decomposition in a semi-arid ecosystem controlled by photodegradation. Nature 442, 555–558.

Barron-Gafford, G.A., Angert, A.L., Venable, D.L., Tyler, A.P., Gerst, K.L., Huxman, T.E., 2013. Photosynthetic temperature responses of co-occurring desert winter annuals with contrasting resource-use efficiencies and different temporal patterns of resource utilization may allow for species coexistence. Journal of Arid Environments 91, 95-103.

Bégué, A., Hanan, N.P., Prince, S.D., 1994. Radiative transfer in shrub savanna sites in Niger: preliminary results from HAPEX-Sahel. 2. Photosynthetically active radiation interception of the woody layer. Agric. For. Meteorol. 69, 247–266.

Belnap, J., Budel, B., Lange, O.L., 2003. Biological soil crusts: characteristics and distribution. In: Belnap, J., Lange, O.L. (Eds.), Biological Soil Crusts: Structure, Function, and Management, vol. 150. Springer, Berlin, pp. 3–30.

Bloemen, J., McGuire, M.A., Aubrey, D.P., Teskey, R.O., Steppe, K., 2013. Transport of root-derived CO2 via the transpiration stream affects aboveground carbon assimilation and CO_2 efflux in trees. New Phytologist 197, 555–565.

Bloemen, J., Teskey, R.O., McGuire, M.A., Aubrey, D.P., Steppe, K., 2016. Root xylem CO_2 flux: an important but unaccounted-for component of root respiration. Trees 30, 343–352.

Bowling, D.R., Grote, E.E., Belnap, J., 2011. Rain pulse response of soil CO_2 exchange by biological soil crusts and grasslands of the semiarid Colorado Plateau, United States. Journal of Geophysical Research G: Biogeosciences 116, 1–17. doi:10.1029/2011JG001643

Bradford, M.A., Wieder, W.R., Bonan, G.B., Fierer, N., Raymond, P.A., Crowther, T.W., 2016. Managing uncertainty in soil carbon feedbacks to climate change. Nature Climate Change 6, 751–758.

Brandt, L.A., King, J.Y., Hobbie, S.E., Milchunas, D.G., Sinsabaugh, R.L., 2010. The role of photodegradation in surface litter decomposition across a grassland ecosystem precipitation gradient. Ecosystems 13, 765–781.

Buysse, P., Goffin, S., Carnol, M., Malchair, S., Debacq, A., Longdoz, B., Aubinet M., 2013. Short-term temperature impact on soil heterotrophic respiration in limed agricultural soil samples. Biogeochemistry 112, 441–455.

Butcher, John C. (2003), Numerical Methods for Ordinary Differential Equations, New York: John Wiley & Sons, ISBN 978-0-471-96758-3.

Chamizo, S., Stevens, A., Canton, Y., Miralles, I., Domingo, F., Van Wesemael, B., 2012. Discriminating soil crust type, development stage and degree of disturbance in semiarid environments from their spectral characteristics. Eur. J. Soil Sci. 63, 42–53.

Caylor, K.K., Scanlon, T.M., Rodríguez-Iturbe, I., 2008. Ecohydrological optimizationof pattern and processes in water-limited ecosystems. In: Water and the Environment: Proceedings of the Workshop in the Vatican Academy of Sciences, November 2005. Vatican Academy of Sciences: Vatican Press: TheVatican.

Castillo-Monroy, A.P., Bowker, M.A., Maestre, F.T., Rodríguez-Echeverría, S., Martinez, I., Barraza-Zepeda, C.E., Escolar, C., 2011. Relationships between biological soil crusts, bacterial diversity and abundance, and ecosystem functioning: insights from a semi-arid Mediterranean environment. Journal of Vegetation Sciences 22:165–174

Chen, J.M., Liu, J., Cihlar, J., Goulden, M.L., 1999. Daily canopy photosynthesis modelthrough temporal and spatial scaling for remote sensing applications. Ecological Modelling 124, 99–119.

876 Chen, X., Duan, Z., 2009. Changes in soil physical and chemical properties during reversal of
877 desertification in Yanchi County of Ningxia Hui autonomous region, China. Environmental Geology
878 57, 975–985.

879 Ciais, P., Sabine, C., Bala, G., Bopp, L., Brovkin, V., Canadell, J., Chhabra, A., DeFries, R.,
880 Galloway, J., Heimann, M., Jones, C., Le Quéré, C., Myneni, R.B., Piao, S., Thornton, P., France,
881 P.C., Willem, J., Friedlingstein, P., Munhoven, G., 2013. Carbon and other biogeochemical cycles. In:
882 Stocker, T., Qin, D., Plattner, G., Tignor, M., Allen, S., Boschung, J., Nauels, A., Xia, Y., Bex, V.,
883 Midgley, P. (Eds.), Climate change 2013—the physical science basis. Cambridge University Press,
884 Cambridge, pp 465–570.

885 Curiel Yuste, J., Baldocchi, D.D., Gershenson, A., Goldstein, A., Misson, L., Wong, S., 2007.
886 Microbial soil respiration and its dependency on carbon inputs, soil temperature and moisture. Global
887 Change Biology 13, 1–18.

888 Curiel Yuste, J., Janssens, I.A., Carrara, A., Ceulemans, R., 2004. Annual Q10 of soil respiration
889 reflects plant phenological patterns as well as temperature sensitivity. Global Change Biology 10,
890 161–169.

891 Domingo, F., Villagarcía, L., Brenner, A.J., Puigdefábregas, J., 2000. Measuring and modeling the
892 radiation balance of a heterogeneous shrubland. Plant Cell and Environment 23, 27–38.

893 Donat, M.G., Lowry, A.L., Alexander, L.V., O'Gorman, P.A., Maher, N., 2016. More extreme
894 precipitation in the world's dry and wet regions. Nature Climate Change 6, 508–513.

895 Emmerich, E.W., 2003. Carbon dioxide flux in a semiarid environment with high carbonate soils.
896 Agricultural and Forest Meteorology 116, 91–102.

897 Fa, K., Liu, J., Zhang, Y., Wu, B., Qin, S., Feng, W., Lai, Z., 2014. CO_2 absorption of sandy soil
898 induced by rainfall pulses in a desert ecosystem. Hydrological Processes 29, 2043–2051.

899 Fan, Z., Neff, J.C., Hanan, N.P., 2015. Modeling pulsed soil respiration in an African savanna
900 ecosystem. Agricultural and Forest Meteorology 200, 282–292.

901 Fang, C., Moncrieff, J.B., 1999. A model for soil CO2 production and transport 1: Model
902 development. Agricultural and Forest Meteorology 95, 225–236.

903 Felde, V.J.M.N.L., Peth, S., Uteau-Puschmann, D., Drahorad, S.L., Felix-Henningsen, P., 2014. Soil
904 microstructure as an under-explored feature of biological soil crusts hydrological properties: case
905 study from the NW Negev Desert. Biodivers Conserv 23, 1687–1708.

906 Feng, W., Zhang, Y., Wu, B., Zha, T., Jia, X., Qin, S., Shao, C., Liu,J., Lai, Z., Fa, K., 2013. Influence
907 of disturbance on soil respiration in biologically crusted soil during the dry season, The Scientific
908 World J. doi:10.1155/2013/408560

909 Feng, W., Zhang, Y., Wu, B., Qin, S., Lai, Z., 2014. Influence of environmental factors on carbon
910 dioxide exchange in biological soil crusts in desert areas. Arid Land Research and Management 28,
911 186–196.

912 Evans, S.E., Wallenstein, M.D., 2011. Soil microbial community response to drying and rewetting
913 stress: does historical precipitation regime matter? Biogeochemistry 109, 101–116.

914 Fu, S., Cheng, W., Susfalk, R., 2002. Rhizosphere respiration varies with plant species and phenology:
915 A greenhouse pot experiment. Plant and Soil 239, 133–140.

916 Gao, Y., Li, X., Liu, L., Jia, R., Yang, H., Li, G., Wei, Y., 2012. Seasonal variation of carbon
917 exchange from a revegetation area in a Chinese desert. Agricultural and Forest Meteorology 156,
918 134–142.

919 Garcia-Pichel, F., Felde, V.J.M.N.L., Drahorad, S., Weber, B., 2016. Microstructure and weathering
920 processes within biological soil crusts. In: Weber, B., Büdel, B., Belnap, J. (Eds.), Biological soil
921 crusts: an organizing principle in drylands. Springer, Switzerland, pp 237–252.

922 Garcia-Pichel, F., Pringault, O., 2001. Microbiology—cyanobacteria track water in desert soils.
923 Nature 413, 380–381.

924 Giardina, C.P., Litton, C.M., Crow, S.E., Asner, G.P., 2014. Warming-related increases in soil CO2
925 efflux are explained by increased below-ground carbon flux. Nature Climate Change 4, 822–827.

926 Gliksman, D., Rey, A., Seligmann, R., Dumbur, R., Sperling, O., Navon, Y., Haenel, S., Angelis, P.D.,
927 Arnone III, J.A., Grünzweig, J.M., 2016. Biotic degradation at night, abiotic degradation at day:
928 positive feedbacks on litter decomposition in drylands. Global Change Biology, doi:
929 10.1111/gcb.13465.

930 Gong, J., Kellomäki, S., Shurpali, N.J., Wang, K., Hyvönen, N., Zhang, C., Zhong, Q., Martikainen,
931 P.J., 2014. Climatic sensitivity of the CO_2 flux in a cutaway boreal peatland cultivated with a
932 perennial bioenergy crop (*Phalaris arundinaceae, L.*): Beyond diplotelmic modeling. Agricultural and
933 Forest Meteorology 198-199, 232-249.

934 Gong, J., Kellomäki, S., Wang, K., Zhang, C., Shurpali, N., Martikainen, P.J., 2013. Modeling CO_2
935 and CH_4 flux changes in pristine peatlands of Finland underchanging climate conditions. Ecological
936 Modelling 263, 64–80.

Gong, J., Jia, X., Zha, T., Wang, B., Kellomäki, S., Peltola, H., 2016. Modelling the effects of plant-interspace heterogeneity on water-energy balances in a semiarid ecosystem. Agricultural and Forest Meteorology 221, 189–206.

Green, T.G.A., Proctor, M.C.F., 2016. Physiology of photosynthetic organisms within biological soil crusts: Their adaptation, flexibility, and plasticity. In: Weber, B., Büdel, B., Belnap, J. (Eds.), Biological soil crusts: an organizing principle in drylands. Springer, Switzerland, pp 347–384.

Henry, H.A.L., Brizgys, P., Field, C.B., 2008. Litter decomposition in California annual grassland: interactions between photodegradation and litter layer thickness. Ecosystems 11, 545–554.

Jarvis, P., Rey, A., Petsikos, C., Wingate, L., Rayment, M., Pereira, J., Banza, J., David, J., Miglietta, F., Borghetti, M., Manca, G., Valentini, R., 2007. Drying and wetting of Mediterranean soils stimulates decomposition and carbon dioxide emission: the "Birch effect". Tree Physiology 27, 929-40.

Jia, R.L., Li, X.R., Liu, L.C., Gao, Y.H., Li, X.J., 2008. Responses of biological soil crusts to sand burial in a revegetated area of the Tengger desert, northern china. Soil Biology and Biochemistry 40:2827–2834

Jia, X., Zha, T.S., Wu, B., Zhang, Y.Q., Gong, J.N., Qin, S.G., Chen, G.P., Qian, D.,Kellomäki, S., Peltola, H., 2014. Biophysical controls on net ecosystem CO2exchange over a semiarid shrubland in northwest China. Biogeosciences 11, 4679–4693.

Jia, X., Zha, T.S., Gong, J.N., Wu, B., Zhang, Y.Q., Qin, S.G., Chen, G.P., Feng, W.,Kellomäki, S., Peltola, H., 2015. Energy partitioning over a semi-arid shrubland in northern China. Hydrological Processes http://dx.doi.org/10.1002/hyp.10685.

Jia, X., Zha, T.S., Gong, J., Wang, B., Zhang, Y., Wu, B., Qin, S, Peltola, H., 2016. Carbon and water exchange over a temperate semi-arid shrub land during three years of contrasting precipitation and soil moisture patterns. Agricultural and Forest Meteorology 228, 120–129.

Karhu, K., Auffret, M.D., Dungait, J.A.J., Hopkins, D.W., Prosser, J.I., Singh, B.K., Subke, J.-A., Wookey, P.A., Ågren, G.I., Sebastià, M.-T., Gouriveau, F., Bergkvist, G., Meir, P., Nottingham, A.T., Salinas, N., Hartley, L.P., 2014. Temperature sensitivity of soil respiration rates enhanced by microbial community response. Nature 513, 81–84.

Kinast, S., Ashkenazy, Y., Meron, E., 2014. A coupled vegetation-crust model for patchy landscapes. Pure and Applied Geophysics 173, 1-11.

Lai, Z., Zhang, Y., Liu, J., Wu, B., Qin, S., Fa, K., 2016. Fine-root distribution, production, decomposition, and effect on soil organic carbon of three revegetation shrub species in northwest China. Forest Ecology and Management 359, 381-388.

970 Lange, O.L., 2003. Photosynthetic productivity of the epilithic lichen *Lecanora muralis*: long-term
971 field monitoring of CO2 exchange and its physiological interpretation. III. Diel, seasonal, and annual
972 carbon budgets. Flora 198, 277–292.

973 Li, Y., Wang, Y., Houghton, R.A., Tang, L., 2015. Hidden carbon sink beneath desert. Geophysical
974 Research Letters 42, 5880–5887.

975 Liu, J., Zhang, Y., Wu, B., Qin, S., Jia, X., Fa, K., Feng, W., Lai, Z., 2015. Effect of vegetation
976 rehabilitation on soil carbon and its fractions in Mu Us desert, northwest China. International Journal
977 of Phytoremediation 17, doi:10.1080/15226514.2014.922923

978 Liu, L.C., Li, S.Z., Duan, Z.H., Wang, T., Zhang, Z.S., Li, X.R., 2006. Effects of microbiotic crusts
979 on dew deposition in the restored vegetation area at Shapotou, northwestern China. Journal of
980 Hydrology 328, 331–337.

981 Liu, P., Zha, T., Jia, X., Wang, B., Guo, X., Zhang, Y., Wu, B., Yang, Q., Peltola, H., 2016. Diurnal
982 freeze-thaw cycles modify winter soil respiration in a desert shrub-land ecosystem. Forests 7,
983 doi:10.3390/f7080161

984 Ma, Q., Cheng, F., Liu, Y., Wang, F., Zhang, D., Jin, H., 2011. Spatial heterogeneity ofsoil water
985 content in the reversion process of desertification in arid areas. Journal of Arid Land 3, 268–277.

986 Ma, J., Wang, Z.Y., Stevenson, B.A., Zheng, X.J., Li, Y., 2013. An inorganic CO_2 diffusion and
987 dissolution process explains negative CO2 fluxes in saline/alkaline soils. Scientific Report 3, doi:
988 10.1038/srep02025.

989 Maier, M., Schack-Kirchner, H., Hildebrand, E.E., Schindler, D., 2011. Soil CO_2 efflux vs. soil
990 respiration: Implications for flux models. Agricultural and Forest Meteorology 151, 1723–1730.

991 Maestre, F.T., Cortina, J., 2003. Small-scale spatial variation in soil CO2 efflux in a Mediterranean
992 semiarid steppe. Applied Soil Ecology 23, 199–209.

993 Maestre, F.T., Escolar, C., Bardgett, R.D., Dungait, J.A., Gozalo, B., Ochoa, V., 2015. Warming
994 reduces the cover and diversity of biocrust-forming mosses and lichens, and increases the
995 physiological stress of soil microbial communities in a semi-arid *Pinus halepensis* plantation. Front
996 Microbial. 6, doi:10.3389/fmicb.2015.00865

997 Maestre, F.T., Escolar, C., Ladrón de Guevara, M., 2013. Changes in biocrust cover drive carbon
998 responses to climate change in drylands. Global Change Biology 19, 3835–3847.

999 Rietkerk, M., Dekker, S.C., de Ruiter, P.C., van de Koppe, J., 2004. Self-organizedpatchiness and
1000 catastrophic shifts in ecosystems. Science 305, 1926–1929.

1001 Reynolds, J.F., Virginia, R.A., Kemp, P.R., de Soyza, A.G., Tremmel, D.C., 1999. Impact of drought
1002 on desert shrubs: effects of seasonality and degree of resource island development. Ecol. Monogr. 69,
1003 69–106.

1004 Phillips, C.L., Nickerson, N., Risk, D., Bond, B.J., 2011. Interpreting diel hysteresis between soil
1005 respiration and temperature. Global Change Biology 17, 515–527.

1006 Pointing, S.B., Belnap, J., 2012. Microbial colonization and controls in dryland systems. Nature
1007 Review Microbiology 10, 551–562.

1008 Rango, A., Tartowskia, S.L., Lalibertea, A., Wainwright, J., Parsons, A., 2006. Islands of
1009 hydrologically enhanced biotic productivity in natural and managed arid ecosystems. J. Arid Environ.
1010 65, 235–252.

1011 Porada, P., Weber, B., Elbert, W., Pöschl, U., Kleidon, A., 2013. Estimating global carbon uptake by
1012 lichens and bryophytes with a process-based model. Biogeosciences 10, 6989–7033.

1013 Poulter, B., Frank, D., Ciais, P., Myneni, R. B., Andela, N., Bi, J., Broquet, G., Canadell, J. G.,
1014 Chevallier, F., Liu, Y. Y., Running, S. W., Sitch, S., van der Werf, G.R., 2014. Contribution of
1015 semiarid ecosystems to interannual variability of the global carbon cycle. Nature, 509, 600–603.

1016 Qi, F., Kunihikow, E., Guodong C., 2002. Soil water and chemical characteristics of sandy soils and
1017 their significance to land reclamation. Journal of Arid Environments 51, 35–54.

1018 Raanan, H., Felde, V.J.M.N.L., Peth, S., Drahorad, S., Ionescu, D., Eshkol, G., Treves, H., Felix-
1019 Henningsen, P., Berkowicz, S., Keren, N., Horn, R., Hagemann, M., Kaplan, A., 2016. Three-
1020 dimensional structure and cyanobacterial activity within a desert biological soil crust. Environ
1021 Microbiol 18, 372–383. doi:10.1111/1462-2920.12859

1022 Raich, J.W., Tufekciogul, A., 2000. Vegetation and soil respiration: correlations and controls.
1023 Biogeochemistry 48, 71-90.

1024 Raich, J.W., Potter, C.S., Bhagawati, D., 2002. Interannual variability in global soil respiration, 1980–
1025 94. Global Change Biology 8, 800–812.

1026 Rastud, L.E., Huntington, T.G., Boone, R.D., 2000. Controls on soil respiration: implications for
1027 climate change. Biogeochemistry 48, 1–6.

1028 Rey, A., Petsikos, C., Jarvis, P.G., Grace, J., 2005. Effect of temperature and moisture on rates of
1029 carbon mineralization in a Mediterranean oak forest soil under controlled and field conditions.
1030 European Journal of Soil Science 56, 589–599.

1031 Reynolds, J.F., Virginia, R.A., Kemp, P.R., de Soyza, A.G., Tremmel, D.C., 1999. Impact of drought
1032 on desert shrubs: effects of seasonality and degree of resource island development. Ecol. Monogr. 69,
1033 69–106.

1034 Rietkerk, M., Dekker, S.C., de Ruiter, P.C., van de Koppe, J., 2004. Self-organized patchiness and
1035 catastrophic shifts in ecosystems. Science 305, 1926–1929.

1036 Rodríguez-Iturbe, I., Porporato, A., Laio, F., Ridolfi, L., 2001. Plants in water-controlled ecosystems:
1037 active role in hydrologic processes and response to water stress—i. Scope and general outline.
1038 Advances in Water Resources 24, 695–705.

1039 Rango, A., Tartowskia, S.L., Lalibertea, A., Wainwright, J., Parsons, A., 2006. Islandsof
1040 hydrologically enhanced biotic productivity in natural and managed aridecosystems. J. Arid Environ.
1041 65, 235–252.

1042 Ryan, M.G., Law, B.E., 2005. Interpreting, measuring, and modeling soil respiration.
1043 Biogeochemistry 73, 3–27.

1044 Sala, O.E., Gherardi, L.A., Reichmann, L., Jobbágy, E., Peters, D., 2012. Legacies of precipitation
1045 fluctuations on primary production: theory and data synthesis. Philos. T. Roy. Soc. B. 367, 3135–3144.

1046 Sancho, L.G., Belnap, J., Colesie, C., Raggio, J., Weber, B., 2016. Carbon budgets of biological soil
1047 crusts at micro-, meso-, and global scales. In: Weber, B., Büdel, B., Belnap, J. (Eds.), Biological soil
1048 crusts: an organizing principle in drylands. Springer, Switzerland, pp 287–304.

1049 Schlesinger, W.H., Belnap, J., Marion, G., 2009. On carbon sequestration in desert ecosystems.
1050 Global Change Biology 15, 1488–1490.

1051 Shen, W., Jenerette, G.D., Hui, D., Scott, R.L., 2016. Precipitation legacy effects on dryland
1052 ecosystem carbon fluxes: direction, magnitude and biogeochemical carryovers. Biogeosciences 13,
1053 425–439.

1054 Šimunek, J., Suarez, D.L., 1993. Modeling of carbon dioxide transport and production in soil: 1.
1055 Model development. Water Resources Research 29, 487–497.

1056 Smith, J.U., Gottschalk, P., Bellarby, J., Chapman, S., Lilly, A., Towers, W., Bell, J., Coleman, K.,
1057 Nayak, D., Richards, M., Hillier, J., Flynn, H., Wattenbach, M., Aitkenhead, M., Yeluripati, J.,
1058 Farmer, J., Milne, R., Thomson, A., Evans, C., Whitmore, A., Falloon, P., Smith, P., 2010. Estimating
1059 changes in national soil carbon stocks using ECOSSE-a new model that includes upland organic soils.
1060 Part I. Model description and uncertainty in national scale simulations of Scotland. Climate Research,
1061 45, 179–192.

1062 Shi, R., Yang, X., Zhang H., Wang, L., 2013. Vertical differentiation analysis of sierozem profile
1063 characteristics in Yili-River valley, China. African Journal of Agricultural Research 8, 6509–6517.

1064 Song, W.M., Chen, S., Zhou, Y., Wu, B., Zhu, Y., Lu, Q., Lin, G., 2015. Contrasting diel hysteresis
1065 between soil autotrophic and heterotrophic respiration in a desert ecosystem under different rainfall
1066 scenarios. Scientific Report 5, doi:10.1038/srep16779

1067 Sponseller, R.A., 2007. Precipitation pulses and soil CO_2 flux in a Sonoran Desert ecosystem, Global
1068 Change Biol., 13(2), 426–436, doi:10.1111/j.1365-2486.2006.01307.x.

1069 Throop, H.L., Archer, S.R., 2009. Resolving the dryland decomposition conundrum: some new
1070 perspectives on potential drivers. Progress in botany. vol. 70. Springer Berlin Heidelberg, 171-194.

1071 Vanderbilt, K.L., White, C.S., Hopkins, O., Craig, J.A., 2008. Aboveground decomposition in arid
1072 environments: results of a long-term study in central New Mexico. Journal of Arid Environments 72,
1073 696–709.

1074 van Gestel, N., Reischke ,S., Bååth, E., 2013. Temperature sensitivity of bacterial growth in a hot
1075 desert soil with large temperature fluctuations. Soil Biology & Biochemistry 65, 180-185.

1076 Viterbo, P., Beljaars, A., Mahfouf, J., Teixeira, J., 1999. The representation of soil moisture freezing
1077 and its impact on the stable boundary layer. Q. J. R. Meteorol. Soc. 125, 2401–2426.

1078 Wang, B., Zha, T.S., Jia, X., Wu, B., Zhang, Y.Q., Qin, S.G., 2014a. Soil moisture modifies the
1079 response of soil respiration to temperature in a desert shrub ecosystem. Biogeosciences 11, 259–268.

1080 Wang, W., Chen, Xi., Luo, G., Li, L., 2014b. Modeling the contribution of abiotic exchange to CO_2
1081 flux in alkaline soil of arid areas. Journal of Arid Land 6, 27–36.

1082 Wang, B., Zha, T.S., Jia, X., Gong, J.N., Wu, B., Bourque, C.P.A., Zhang, Y., Qin, S.G., Chen, G.P.,
1083 Peltola, H., 2015. Microtopographic variation in soil respiration and its controlling factors vary with
1084 plant phenophases in a desert-shrub ecosystem. Biogeosciences 12, 5705–5714.

1085 Williams, A.J., Buck, B.J., Beyene, M.A., 2012. Biological soil crusts in the Mojave desert, USA:
1086 micromorphology and pedogenesis. Soil Science Society of America Journal 76, 1685–1695.

1087 Xie, J.X., Li, Y., Zhai, C.X., Lan, Z., 2009. CO_2 absorption by alkaline soils and its implication to the
1088 global carbon cycle. Environmental Geology 56, 953–961.

1089 Xu, L., Baldocchi, D., Tang, J., 2004. How soil moisture, rain pulses, and growth alter the response of
1090 ecosystem respiration to temperature. Global Biogeochemical Cycles 18, doi: 10.1029/2004GB00228.

1091 Yanai, R., 1994. A steady-state model of nutrient uptake accounting for newly grown roots. Soil. Sci.
1092 Soc. Am. J. 58, 1562-1571.

Zaady, E., Kuhn, U., Wilske, B., Sandoval-Soto, L., Kesselmeier, J., 2000. Patterns of CO_2 exchange in biological soil crusts of successional age. Soil Biology and Biochemistry 32, 959–966.

Zhang, J., Hou, P., 2012. Changes in soil properties during reversal of desertification in agro-pastoral transition zone of Northern China. African Journal of Agricultural Research 7, 3284-3292.

Zhang, Z.S., Li, X.R., Wang, T., Wang, X.P., Xue, Q.W., Liu, L.C., 2008. Distribution and seasonal dynamics of roots in a revegetated stand of *Artemisia ordosica* Kracsh. in the Tengger Desert (North China). Arid Land Res. Manag. 22, 195–211.

Tables

Table 1. Configuration of soil collars used in this study

Collars	C1	C2	C3
Surface type	Non-crusted	Lichen-crusted	Lichen-crusted
Chamber type	Opaque	Opaque	Transparent
Root biomass (g m^{-3})	420	106	92
Gap of data (%)	12.9	10.5	9.85
Annual C efflux (gC m^{-2}) [a]	259	194	192

[a] The values were calculated from the measured hourly FS data excluding data gaps.

Table 2. Parameters for soil water retention and C turnover

Parameter	Equation	Unit	Value
α_h	- [a]	-	0.0355 [b]
n	- [a]	-	1.5215 [b]
k_1	(11)	g g^{-1} day^{-1}	0.01 [c]
k_2	(11)	g g^{-1} day^{-1}	0.08 [d]
k_3	(11)	g g^{-1} day^{-1}	0.001 [d]
k_g	(15)	g g^{-1}	0.15 [e]
k_{cr}	(19)	g g^{-1} s^{-1}	0.0014 [f]

k_p	(24)	g g^{-1} year^{-1}	0.23 [g]
k_{R0}	(25)	g g^{-1} day^{-1}	0.002 [e]
a	(26)	-	0.1 [h]
b	(26)	-	24 [h]
c	(26)	-	0.89 [h]
Q_{Ct}	(32)	-	1.585 [f]
a_{RC}	(32)	-	-0.0525 [f]
b_{RC}	(32)	-	2.602 [f]
c_{RC}	(32)	-	-1.653 [f]
a_{Pt}	(33)	-	0.9837 [f]
b_{Pt}	(33)	-	-0.1385 [f]
c_{Pt}	(33)	-	0.0095 [f]
d_{Pt}	(33)	-	-1.6318E-4 [f]
a_{Pw}	(33)	-	-0.3501 [f]
b_{Pw}	(33)	-	5.5884 [f]
c_{Pw}	(33)	-	-7.1783 [f]
d_{Pw}	(33)	-	2.6837 [f]

[a] See Eq. (26) in Gong et al. (2016). Sources of parameter values: [b] This study, see section 2.3.2; [c] Lai et al. (2016); [d] Gong et al. (2014); [e] Chen et al. (1999); [f] This study, see section 2.4.4 and Fig. 3; [g] Wang et al., 2014a.

Table 3. Simulated component CO_2 fluxes (gC m^{-2} year^{-1}) for areas with plant cover and without (interspace).

Surface type	F_S	F_T	$Rs+Ra$ [a]	Ra	P_{Ct}	F_{Ct}	F_P	F_{Ct} - F_P [b]
Interspace	244	249	295	113	54.6	31.1	26.1	5.0
Plant covered	214	218	263	108	36.3	18.2	14.6	3.6

[a] $Rs+Ra$ represents the total CO_2 production from soil respirations. Ra is the total autotrophic respiration ($Ra = \sum_i Ra_i$, see Eq. (10)) and Rs is the total heterotrophic respiration ($Rs = \sum_i Rs_i$, see Eq. (12)); [b] F_{Ct} - F_P represents the net CO_2 exchanges of topcrust, see Eq. (17) and Eq. (24) for correspondent algorithms of the variables. For definitions of other fluxes, see Eq. (1) for F_S, Eq. (3) for F_T, Eq. (17) for F_{Ct}, Eq. (18) for P_{Ct} and Eq. (24) for F_P.

Table 4. Sensitivity of simulated F_S and its componential fluxes to manipulations of parameter values.

Change of parameter	F_S [a]	F_T	$Ra+R_S$	Ra	P_{Ct}	F_{Ct}	F_P	F_{Ct} - F_P
n_R +20 %	+3.3 [b]	+3.2	+2.7	+7.9	/ [c]	/	/	/
n_R -20 %	-2.9	-2.8	-3.4	-8.8	/	/	/	/
n_P +20 %	+1.6	+1.6	+1.0	/	/	/	/	/
n_P -20 %	/	/	-1.4	/	/	/	/	/
f_m +20 %	/	/	/	/	+2.9	+3.8	+3.4	+6.0
f_m -20 %	/	/	/	/	+1.2	/	-5.7	+30
Ts +2 ºC	+9.5	+9.6	+7.1	+11	+4.9	+3.9	+1.5	+16

Ts -2 ºC	-9.0	-9.2	-8.1	-11	-1.3	-2.9	/	-20
θ +10 %	+3.6	+5.6	+7.5	+14	+41	+28	+14	+102
θ -10 %	-5.0	-5.6	-8.1	-14	-16	-13	-8.4	-34
M_{tot} +10 %	+2.9	+2.8	+2.0	/	/	/	/	/
M_{tot} -10 %	-2.5	-2.4	-3.1	/	/	/	/	/
M^R +10 %	+7.0	+6.8	+6.8	+8.8	/	/	/	/
M^R -10 %	-7.0	-6.8	-7.1	-8.9	/	/	/	/
N_{tot} +10 %	/	/	/	/	/	/	/	/
N_{tot} -10 %	/	/	/	/	/	/	/	/
k_1 +10 %	+2.9	+2.8	+2.4	/	/	/	/	/
k_1 -10 %	-2.5	-2.4	-3.1	/	/	/	/	/
k_{mo} +10 %	+4.1	+4.0	+3.4	/	/	/	/	/
k_{mo} -10 %	-3.3	-3.2	-3.7	/	/	/	/	/
k_{mc} +10 %	/	/	/	/	/	/	+1.5	-8.0
k_{mc} -10 %	/	/	/	/	/	/	-2.3	+8.0
M_{Ct} +10 %	/	/	/	/	/	/	/	/
M_{Ct} -10 %	/	/	/	/	/	/	/	/
M_{CA}:M_{CH} +10 %	/	/	/	/	/	/	/	/
M_{CA}:M_{CH} -10 %	/	/	/	/	/	/	/	/
pH +5 %	-8.6	-8.4	/	/	/	/	/	/
pH -5 %	+7.0	+6.8	/	/	/	/	/	/

[a] Definitions of fluxes see Table 3 and Section 2.5.3; [b] Value represents the percentage (%) of change (dF) in correspondent C flux with manipulated parameter value, as compared to the no-change condition. A positive value represents the percentage of increase in the simulated flux whereas a negative value represents the percentage of decrease; [c] the change in simulated C flux was smaller than 1 %.

Table 5. Plant-interspace differences in the sensitivities of C fluxes to changes in soil temperature (Ts), water content (θ) and root biomass (M^R).

Change of parameter	F_S [a]	F_T	$Ra+R_S$	Ra	P_{Ct}	F_{Ct}	F_P
Ts +2 ºC	+0.38 [b] (+4.0)	+0.45 (+4.7)	+0.87 (+12)	+0.49 (+4.6)	+1.7 (+34)	+2.7 (+70)	+1.2 (+78)
Ts -2 ºC	-1.6 (+18)	-1.3 (+14)	-0.61 (+7.4)	/ [c]	-2.8 (+222)	-0.40 (+14)	-3.1 (+615)
θ +10 %	-1.8 (-49)	-1.5 (-27)	/	-0.27 (-1.9)	+8.7 (+21)	+13 (+46)	+2.9 (+20)
θ -10 %	+0.84 (-17)	+0.58 (-10)	/	+1.5 (-10)	-3.5 (+22)	-4.5 (+36)	+0.9 (-11)
M^R +10 %	-0.44 (-6.3)	-0.41 (-6.0)	-0.31 (-4.7)	-0.52 (-5.8)	/	/	
M^R -10 %	+0.44 (-6.3)	+0.41 (-6.0)	+0.65 (-9.2)	+5.2 (-5.8)	/	/	

[a] Definitions of fluxes see Table 3 and Section 2.5.3; [b] Values shows the plant-interspace difference in parameter sensitivities by value (outside bracket, dF_p - dF_i) and by percentage (inside bracket, 100 × ($|dF_p|$ - $|dF_i|$) / $|dF_i|$), where dF_p and dF_i are parameter sensitivities (dF, definitions see Table 4 and Section 2.5.3) for

plant-covered and interspace areas, respectively. A positive percentage (inside bracket) indicates a greater sensitivity (|*dF*|) of the flux at plant cover than interspace, whereas a negative value indicates a lower sensitivity. Definitions of fluxes and sensitivities see Table 3 and Section 2.5.3. [c] the difference in sensitivity are smaller than 0.1% by value.

Figures

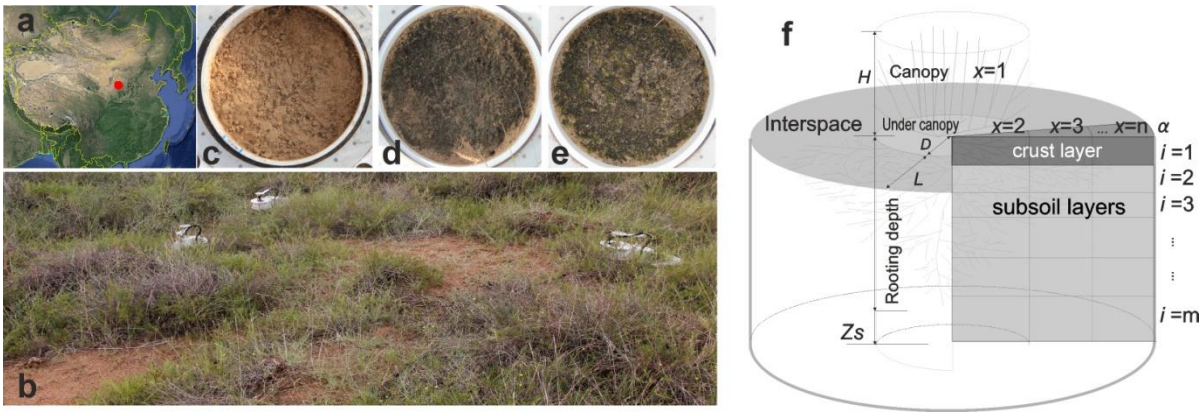

Figure 1. Site position (a), overlook of measured ecosystem (b), appearance of soil surface at collar C1 (c), C2 (d) and C3 (e), and layout of representative land unit (RLU, adopted from Gong et al., 2016)

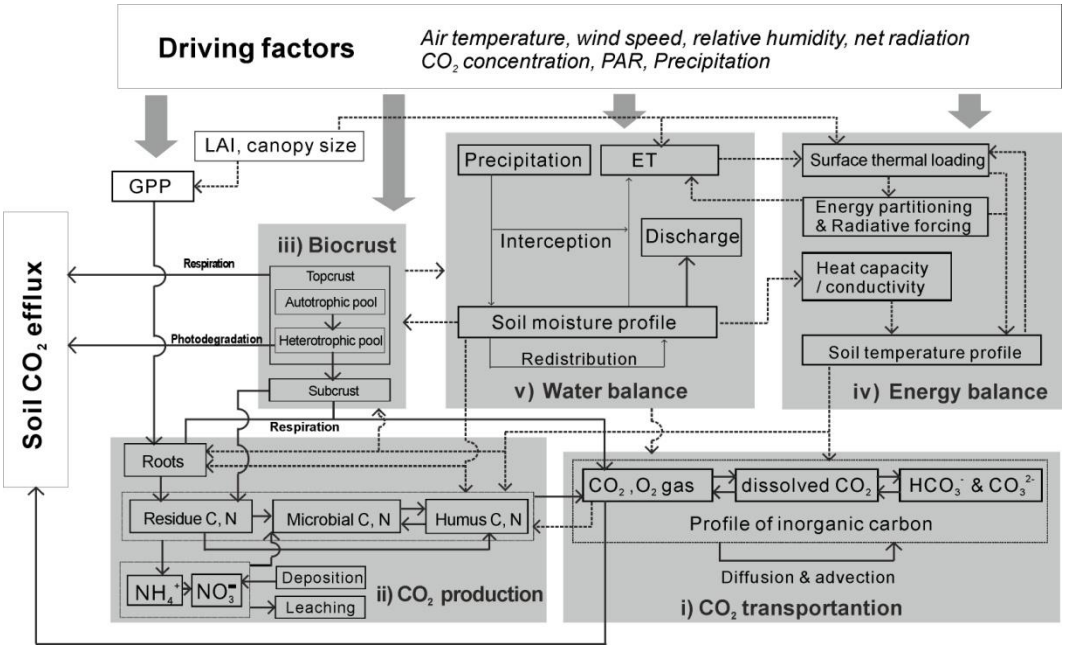

1154

1155 Figure 2. Conceptual framework of process-based modelling. Solid arrows represent flows of masses
1156 and dash arrows represent flows of information.

1157

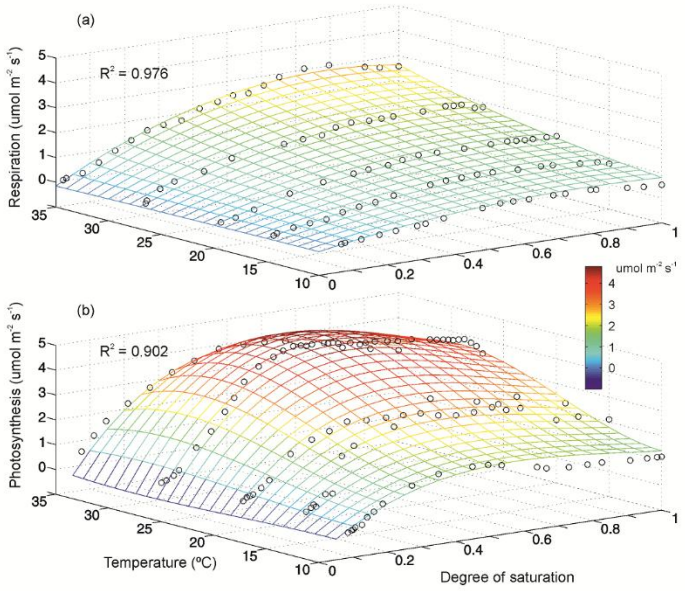

1158

1159 Figure 3. Measured and fitted bulk respiration (a) and photosynthesis (b) of the lichen topcrust as
1160 functions of temperature and water content.

1161

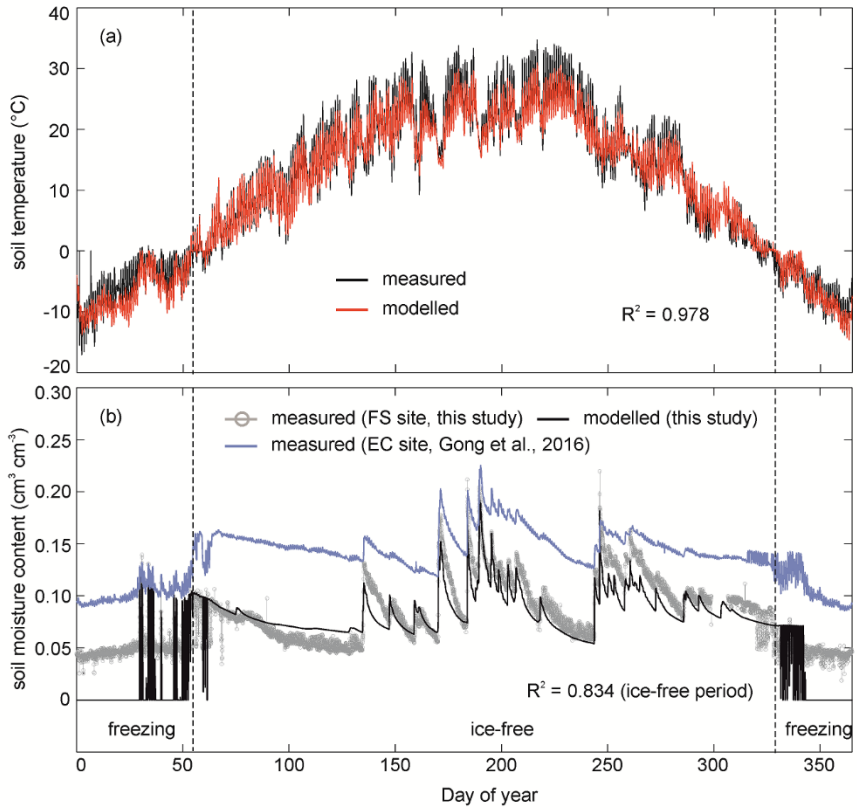

1162

1163 Figure 4. Measured and modelled soil temperature (a) and soil moisture content (b) at 10 cm depth for

1164 F_S site, and as compared to the EC site in year 2013 by Gong et al. (2016).

1165

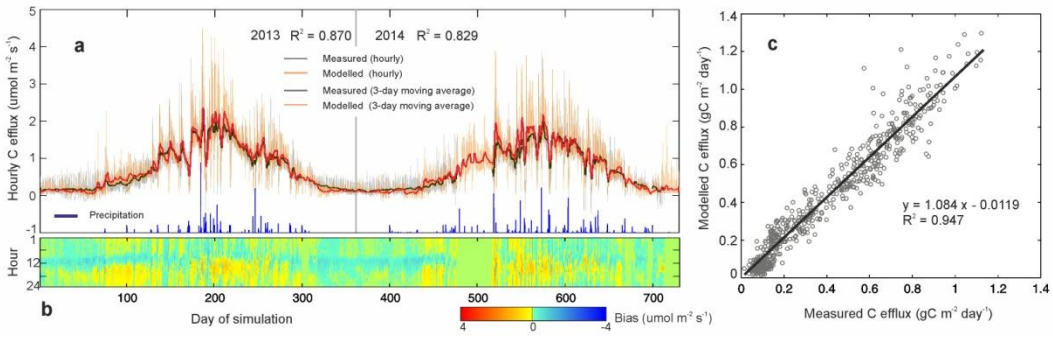

1166

1167 Figure 5. Measured and modelled hourly F_S for non-crusted soil (a), the temporal pattern of the bias of

1168 simulated hourly F_S (b) and the comparison of measured and modelled daily F_S (c) during 2013-2014.

1169

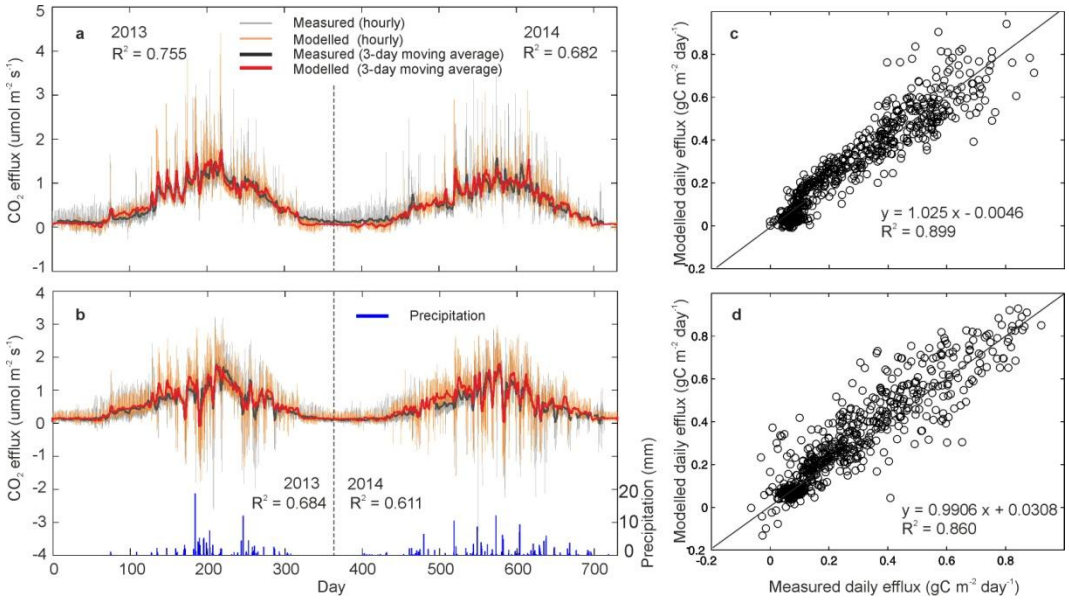

Figure 6. Measured and modelled F_S of lichen-crusted soils for opaque (a, c) and transparent chambers (b, d) at hourly (a, b) and daily (c, d) scales during 2013-2014.

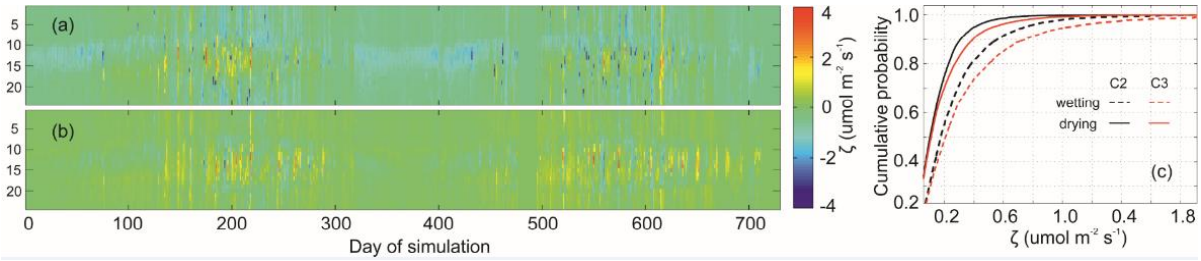

Figure 7. Diurnal patterns of biases (ζ) in the simulated hourly F_S for lichen-crusted soils using opaque (a) and transparent chambers (b), and the cumulative probability of the biases during wetting and drying periods (c) during 2013-2014. The wetting period included the raining days and a 1-day period after each rainfall. The drying period included the rest time of the years other than the wetting period.

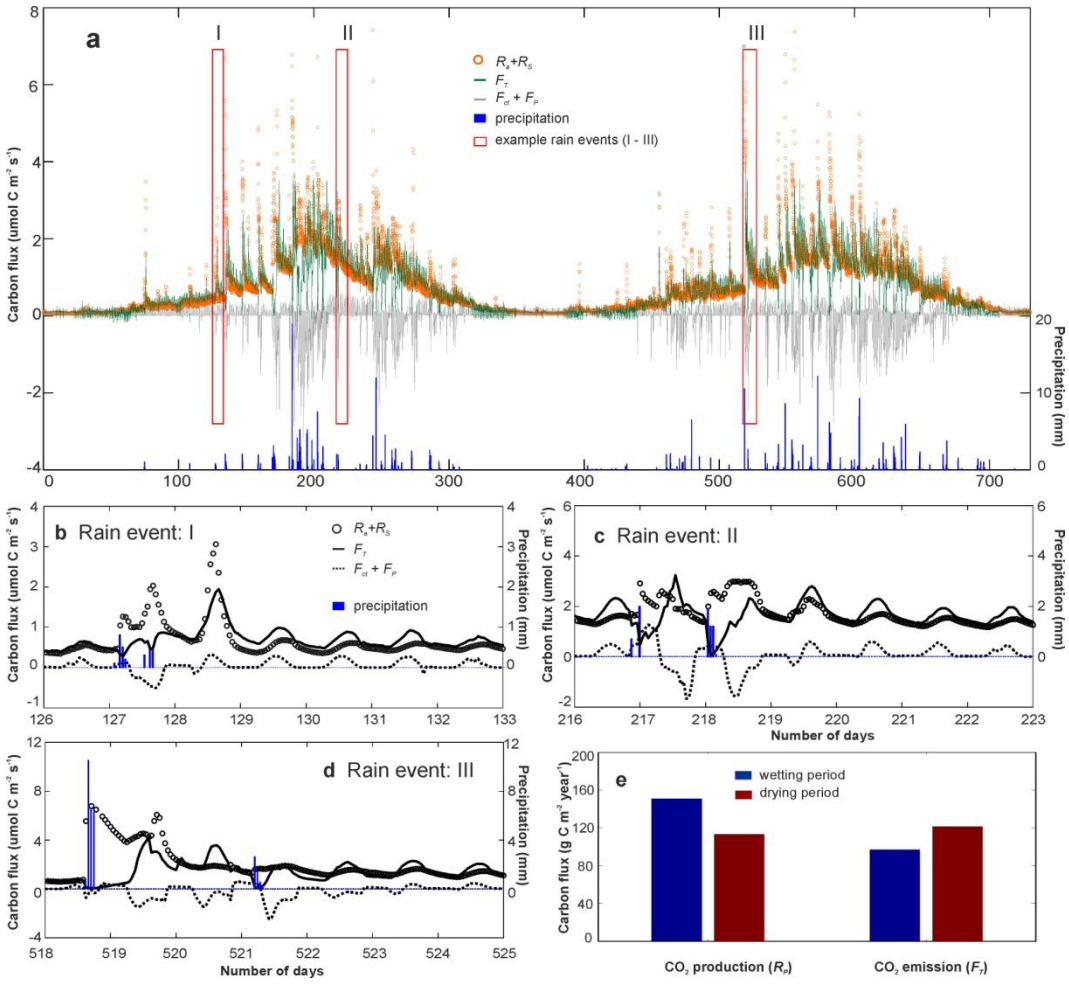

1181

1182 Figure 8. Simulated component CO_2 exchanges by biocrust and root-zone soil (a), the simulated CO_2
1183 fluxes before and after example rain events of 2.3 mm (b), 7.6 mm (c) and 12.8 mm (d) sizes, and the
1184 comparison of F_T and R_R during wetting and drying periods during 2013-2014. The wetting period
1185 included the raining days and a 1-day period after each rainfall. The drying period included the rest
1186 time of the years other than the wetting period.

1187

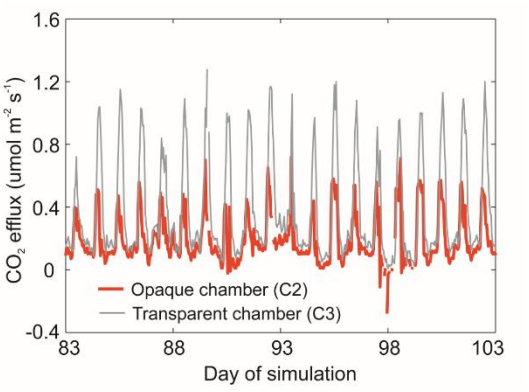

1188

1189 Figure 9. Comparison of the measured F_S from lichen-crusted surfaces using opaque and transparent
1190 chambers during a dry period (day 83-103) in spring 2013.